

AD A049535

AD No. 1
DDC FILE COPY

AFOSR-TR- 77- 1311

AERONUTRONIC FORD PUBLICATION NO. U-6381 ✓

AFOSR TR No.

2
B.S.

LAMINAR BOUNDARY LAYER
STABILITY MEASUREMENTS AT MACH 7
INCLUDING WALL TEMPERATURE EFFECTS

Prepared by
Anthony Demetriades

Ford Aerospace & Communications Corp
Aeronutronic Division
Ford Road
Newport Beach, California
92663

November 1977

Prepared for

U. S. Air Force Office of Scientific Research
Building 410
Bolling Air Force Base
Washington, D.C. 20332

Under Contract

F44620-75-C-0016

AIR FORCE OFFICE OF SCIENTIFIC RESEARCH (AFSC)
NOTICE OF TRANSMITTAL TO DDC
This technical report has been reviewed and is
approved for public release IAW AFR 190-12 (7b).
Distribution is unlimited.
A. D. BLOSE
Technical Information Officer

Approved for public release;
distribution unlimited.

DDC
FEB 2 1978
OFF

19 REPORT DOCUMENTATION PAGE		READ INSTRUCTIONS BEFORE COMPLETING FORM
1. REPORT NUMBER (13) AFOSR TR-37 7-01311 ✓	2. GOVT ACCESSION NO.	3. RECIPIENT'S CATALOG NUMBER
4. TITLE (and Subtitle) (6) LAMINAR BOUNDARY LAYER STABILITY MEASUREMENTS AT MACH 7 INCLUDING WALL TEMPERATURE EFFECTS.	5. TYPE OF REPORT & PERIOD COVERED (9) INTERIM rept. 1 Jul 1976 - 30 Jun 1977	
7. AUTHOR(s) (20) ANTHONY DEMETRIADES	6. PERFORMING ORG. REPORT NUMBER (14) 746381	
9. PERFORMING ORGANIZATION NAME AND ADDRESS FORD AEROSPACE & COMMUNICATIONS CORP AERONUTRONIC DIVISION - FORD ROAD NEWPORT BEACH, CALIFORNIA 92663	8. CONTRACT OR GRANT NUMBER(s) (15) F44620-75-C-0016	
11. CONTROLLING OFFICE NAME AND ADDRESS AIR FORCE OFFICE OF SCIENTIFIC RESEARCH/NA BLDG 410 BOLLING AIR FORCE BASE, D C 20332	10. PROGRAM ELEMENT, PROJECT, TASK AREA & WORK UNIT NUMBERS (16) 2307A2 (17) 1A2 61102F	
14. MONITORING AGENCY NAME & ADDRESS (if different from Controlling Office)	12. REPORT DATE (12) Nov 77	
	13. NUMBER OF PAGES 70 (12) 73P	
	15. SECURITY CLASS. (of this report) UNCLASSIFIED	
16. DISTRIBUTION STATEMENT (of this Report) Approved for public release; distribution unlimited.		
17. DISTRIBUTION STATEMENT (of the abstract entered in Block 20, if different from Report) DDC FORM 1 FEB 2 1976 RESOLVED F		
18. SUPPLEMENTARY NOTES		
19. KEY WORDS (Continue on reverse side if necessary and identify by block number) HYDRODYNAMIC STABILITY HYPERSONIC STABILITY HYDRODYNAMIC STABILITY OF CONES		
20. ABSTRACT (Continue on reverse side if necessary and identify by block number) An experiment was performed to verify and extend earlier observations of instabilities in the hypersonic laminar boundary layer of cones. The present tests were performed at edge Mach number 7 in a continuous wind tunnel, at edge Reynolds numbers from one to three million and wall-to-stagnation temperature ratios of 0.41 to 0.8. Stability data were obtained for non-dimensional frequencies as high as 5×10^{-4} with high data density provided by computerized data reduction techniques, which were also used to re-examine earlier data. The results are consistent with all earlier data and reveal a complex stability diagram with at least three unstable regions. The lower of these regions		

appears to be generated by the first and second mode instabilities but no theoretical guidance exists to help identify the contributing modes for the other regions. The second-mode instability has the highest amplification rates and generates the optically detectable "laminar waves"; a "second harmonic" to these waves is generated by the modes populating the next most prominent unstable region. The stability diagram extends smoothly into the non-linear and transitional regimes, which are marked by the attainment of a maximum amplitude and then a decay, of the laminar waves. Wall cooling causes a substantial increase of the amplification rates with a concurrent upstream movement of the transition zone.

UNCLASSIFIED

SECURITY CLASSIFICATION OF THIS PAGE(When Data Entered)

ABSTRACT

An experiment was performed to verify and extend earlier observations of instabilities in the hypersonic laminar boundary layer of cones. The present tests were performed at edge Mach number 7 in a continuous wind tunnel, at edge Reynolds numbers from one to three million and wall-to-stagnation temperature ratios of 0.41 and 0.8. Stability data were obtained for non-dimensional frequencies as high as 5×10^{-4} with high data density provided by computerized data reduction techniques, which were also used to re-examine earlier data. The results are consistent with all earlier data and reveal a complex stability diagram with at least three unstable regions. The lower of these regions appears to be generated by the first and second mode instabilities but no theoretical guidance exists to help identify the contributing modes for the other regions. The second-mode instability has the highest amplification rates and generates the optically detectable "laminar waves"; a "second harmonic" to these waves is generated by the modes populating the next most prominent unstable region. The stability diagram extends smoothly into the non-linear and transitional regimes, which are marked by the attainment of a maximum amplitude and then a decay, of the laminar waves. Wall cooling causes a substantial increase of the amplification rates with a concurrent upstream movement of the transition zone.

FOREWORD

This report describes a new wind tunnel experiment done by Aeronutronic Division of Ford Aerospace & Communications Corporation to measure stability characteristics of a hypersonic laminar boundary layer. The work is sponsored by the U.S. Air Force Office of Scientific Research (AFOSR) under Contract F44620-75-C-0016. Mr. Milton Rogers and Col. Lowell Ormond of AFOSR deserve thanks for encouraging this research. Thanks are also due Capt. Tom Hopkins and Capt. Craig Jones of USAF/SAMSO for expediting the use of the AEDC facilities for the tests. These facilities consisted of the Wind Tunnel B of AEDC's Von Karman Facility (VKF). Mr. Joseph Donaldson of ARO, Inc., VKF Project Engineer, was most cooperative in preparing and overseeing the wind tunnel tests; a word of gratitude is also due Dr. James Kendall of NASA/JPL for availing the slender cone model on which the measurements were carried out.

The description of the wind tunnel, test matrix, tunnel instrumentation, etc., for this experiment have been thoroughly documented in a separate report issued by ARO, Inc. (AEDC DR-77-62), which also contains all the mean flow boundary layer data acquired in tabular and graphical form. This report has been distributed to the sponsoring agency and should be consulted for details of the test itself.

In addition to the discussion of the present experiment (denoted "BLT-B"), this report also presents new boundary layer stability information from an older experiment, designated TBL-C, performed at AEDC a few years ago. Since the range of conditions of TBL-C supplemented and extended the present range a second look at its results was thought wise, especially since the greatly improved data reduction software since TBL-C was done allowed a far more detailed and accurate data reduction process. As this report will show, the two experiments, jointly considered, now shed considerable light on the stability behavior of the boundary layer.

The large volume of experimental results generated in this work has generated an equally large number of graphs and tables; for example, several hundred plots of amplification rate variation with Reynolds number are on file, of which only a few samples are included in this report so as not to greatly increase the size of the latter. Readers interested in specific cases not shown here should contact the author.

DOCUMENT ID		e Section <input checked="" type="checkbox"/>	
		f Section <input type="checkbox"/>	
		<input type="checkbox"/>	
CLASSIFICATION		CODES	
		SPECIAL	
A			

CONTENTS

	Page
Abstract	ii
Foreword	iii
Table of Contents	iv
List of Symbols	v
List of Figures	vii
1. Introduction	1
2. Facilities and Equipment	2
3. Method of Data Acquisition	2
4. Results of the Mean Flow Measurements	3
5. Principle of the Fluctuation Measurements	3
6. Fluctuation Data Acquisition and Reduction	4
7. Variation of Amplitude and Amplification	6
8. Stability Diagram: Overview	6
9. The Lower Unstable Region	7
10. The Middle Unstable Region	7
11. The Upper Unstable Region	8
12. Amplification Rates	9
13. Maximum Amplitude Laminar Waves	9
14. Freestream Inputs and Boundary Layer Response	10
15. The Non-Linear Regime and Transition to Turbulence	11
16. Summarizing Discussion and Conclusions	13
17. The Need for Additional Data	14
References	22
Figures	23
Appendix: Computer Operations for Data Processing	50

SYMBOLS

A	disturbance rms amplitude (within a certain narrow frequency band) corrected for noise
A ₀	equivalent to A in the freestream
C _i	coefficients of polynomial fit to A = A(R)
e	rms voltage output of hot film probe
E	disturbance rms amplitude not corrected for noise
f	frequency
F	dimensionless frequency = $2\pi f / u_e Re'_e$
G	amplification rate = $-\alpha_i$
K	transfer function connecting disturbance level and probe output
M	Mach number
N	identified Fourier component ($1 < N < 199$ in frequency range chosen)
P	pressure
Q _i	type of flow disturbance (velocity fluctuation, temperature fluctuation, etc.)
Q _{i0}	initial value of Q _i
R	= $\sqrt{Re_x}$
Re	Reynolds number
Re'	unit Reynolds number
Re _x	= $x Re'$ (Reynolds number based on x)
S _i	sensitivity of hot film probe to the Q _i fluctuation
T	temperature
T _t	total temperature (local) measured with the T ₀ probe
T _w	model wall temperature
x	distance along ray from cone apex
y	direction normal to the model surface
u	velocity
$-\alpha_i$	amplification rate = $\frac{1}{2A} \frac{\partial A}{\partial R}$

δ	boundary layer thickness
δ^*	displacement thickness of boundary layer
θ^*	momentum thickness of boundary layer
λ	wavelength of disturbance
ρ	density
ψ^o	orientation of disturbance wavefront relative to flow vector
$()_o$	supply (stagnation) conditions
$()_e$	boundary layer edge conditions
$()_\infty$	freestream conditions

FIGURES

Page

1. Cone model installation in the wind tunnel. Inset shows hot film probe close to the surface with second probe positioned higher to sample simultaneously the freestream turbulence (pitot tube and total temperature probe are not clearly visible).
2. Reynolds number ranges investigated
3. Measured boundary layer profiles with cold wall, laminar flow. Dashed lines represent expected variations near the wall.
4. Laminar and turbulent profiles for both cold and hot wall . .
5. Measured boundary layer thicknesses
6. Typical variation of a Fourier component (in this case $N = 100$ signifies 80 KHz) along the cone surface at $y/\delta = 0.72$. Data (crosses) are least-squares curve fitted by solid line. In this example, an upper neutral branch (entry of the waves into a damped region) occurs at about $R = 1420$. .
7. Typical variation of amplification rate with Reynolds number. Note how the computer automatically provides the neutral branch location at $R = 1160$ (in this case a lower branch) and the coordinates of maximum damping (at $R = 1115$, $-\gamma_i = -0.000407$) and maximum amplification (at $R = 1333$, $-\gamma_i = 0.00282$) . . .
8. Typical amplification rate spectrum, in this case for supply pressure of 160 psia, $T_w = 0.41 T_o$ and $R = 1597$ ($Re_x = 2.55 \times 10^6$). Earlier studies dealt with the left hand half of this spectrum. The middle and upper unstable regions were found in the present experiment.
9. Experimental results on the overall stability diagram with $T_w/T_o = 0.8$
10. Experimental results on the overall stability diagram with $T_w/T_o = 0.41$
11. Experimental results on the lower unstable region in the cold wall case
12. Experimental results on the lower unstable region, hot wall case
13. Fluctuation spectra at $y/\delta = 0.72$, supply pressure of 106 psia and $T_w = 0.41 T_o$. Note the growth of the laminar waves and the emergence of the second harmonic as one proceeds downstream

FIGURES (Continued)

Page

14. Evolution of the amplification spectra $G(F) = \alpha_1(F)$ for the cold (above) and hot (below) wall cases. Spectra at left are for the $R = 1577$. First instability mode is thought to lie between the prominent peak and the ordinate axis
15. Experimental results on the middle unstable region, cold wall case
16. Experimental results on the middle unstable region, hot wall case
17. Effect of wall temperature on the major features of the stability diagram
18. Maximum amplification rates in the lower unstable region (second mode instabilities, $\psi^0 = 0$)
19. Maximum amplification rates in the middle unstable region. Contributing modes are unknown
20. Amplitude spectra (typical)
21. Maximum amplitude lines (of the laminar waves) and their relation to the upper neutral branch of the lower unstable region. Laminar waves damp beyond the crossing point.
22. Length of the laminar waves compared to the boundary layer thickness δ . Note slight increase with streamwise distance and lowered surface temperature
23. Boundary layer response (TBLC, $R = 1166$, $P_0 = 150$ psia).
24. Boundary layer response (TBLC, $R = 1628$, $P_0 = 150$ psia).
25. Boundary layer response (TBLC, $R = 1780$, $P_0 = 350$ psia).
26. Comparison of freestream spectra at $P_0 = 150$ and 350 psia (TBL-C)
27. Maximum amplitude of laminar waves referred to the freestream spectrum
- A.1. Diagram of computations used for data reduction

1. INTRODUCTION

The present work was undertaken in order to produce experimental data on the stability of hypersonic laminar boundary layers and comes in a period of continued search for a physical mechanism to explain boundary layer transition. The importance of the hydrodynamic stability of the flow to transition lies in the notion that small disturbances in the boundary layer can grow in size to the point where they break up into turbulence. If this growth can be predicted, then the break up can possibly also be predicted. Mathematically, the stability problem is extremely complex. A review of stability theory can be made by beginning with the recent summary of Mack⁽¹⁾. Experimental proof of the theory at its various stages has been equally hard to obtain. This work, for example, is the fourth report ever made of stability observations at hypersonic speeds.

Fifteen years of inactivity in boundary layer stability experiments have been ended by the emergence of several coinciding factors. One is the need of a criterion for transition predictions on re-entry vehicles and another the influence of wind tunnel stream noise on transition predictions on wind tunnel models. Experimental hardware and software have become quite sophisticated, while at hypersonic speeds, selectively amplified laminar instabilities are exceptionally clear and easy to detect and measure. Most importantly, the theory¹ has been advanced to the point where the questions asked of the experimentalist are specific, the experimental targets are clearer than ever before, and guidelines helpful to the identification, measurement and interpretation of the data have been set.

Now that the data of References 2 and 3 have shown the appearance of instabilities on a slender cone at $M_e = 7$, five questions become important: 1) What precisely are the stable and unstable regions, i.e., what is the "stability diagram?" 2) How does the stability diagram agree with the linearized theory? 3) What is the role of the freestream disturbances and how they affect the stability characteristics? 4) What happens to the stability diagram towards the large Re_x where non-linearities and transition occur? 5) What is the effect of wall cooling on stability? Of these, the first, fourth and fifth were the subject of the present study. It was felt that before comparisons with theory are launched, there should first be an extensive mapping of the unstable regions at Mach 7 beyond the meager information of References 2 and 3. Furthermore, a recomputation of the data contained in Reference 3 (made possible by playback of the raw data tapes) would enable the mapping of stability to be extended into the transition zone in more detail than before. Finally, wall cooling was included in the present tests to observe its effect on stability.

A minor but interesting addition to the present work was the use of the same cone model as used by Kendall (Reference 2) but in the same wind tunnel as used in Reference 3. By the "mix" of wind tunnel and cone model in these three tests (References 2, 3 and the present work) a check of possible extraneous factors caused by the model or wind tunnel is possible. As we shall see, the results of the three experiments are quite the same thus bolstering faith in the validity of the results.

2. FACILITIES AND EQUIPMENT

A detailed description of the wind tunnel, cone model, tunnel data acquisition system, etc., for this experiment are given in Reference 4. Briefly, the cone model was positioned at zero incidence along the axis of AEDC's Wind Tunnel B which operated continuously at $M_\infty = 8$ and $T_0 = 800^\circ\text{F}$. In both the water-cooled cold wall mode and the hot-wall mode, data were taken only after the model had been exposed to the flow for an hour or more, ensuring thermal equilibration. Monitoring of the surface conditions via thermocouples, static taps and shadow optics was frequent and meticulous. Diagnostics were done by a four-probe rake bearing a pitot tube, a T_0 probe and two hot films - a boundary layer hot film probe (BLHF) and a freestream hot film probe (FSHF). The hot film probes were made at Aeronutronic and showed excellent endurance to the heated tunnel flow. Typical operating conditions for the films are shown on Table I.

The Tunnel B data acquisition system was used to provide the mean flow profiles in near-real-time. The software used in reducing these data includes the iterations necessary to interpret the T_0 probe readings.

It should be emphasized that the freestream turbulence content is known at AEDC/B. The pressure fluctuations generated in this tunnel by radiation from the sidewalls has been plotted by Laderman in comparison with those of other wind tunnels (Reference 5). Laderman's conclusion is that the noise level at AEDC/B is the same, within the data scatter, as that of other research facilities (see Figure 2 of Reference 5). Therefore, there is no reason to expect spurious effects distorting the present data in a manner different from that in other wind tunnels.

3. METHOD OF DATA ACQUISITION

As Reference 5 indicates, two types of data were taken in this experiment: mean flow data and fluctuation data on the stability of the laminar layer. The former were necessary to ensure that the layer was laminar, to fix the transition zone and to measure the boundary layer thickness and its variation with P_0 and T_w . These data were taken by moving the probe rake away from the surface by small increments and taking readings at each stop. The readings were simultaneously recorded and reduced by the Tunnel B computer. The x positions, P_0 levels and T_w levels for these measurements are shown on Table III and described in great detail in Reference 5.

For the fluctuation measurements, the hot film probe was activated at constant current, the probe tips lowered to the model surface and then the entire rake was slowly traversed away from the surface until it reached a position approximately 1.5δ . During the traverse, all probe outputs (hot film probe signals, pitot pressure transducer output, probe position, etc.,) were recorded at 120 ips on analog tape. The hot film channel electronics had an upper frequency cut-off at 400 KHz (broadband FM) which is sufficiently wide to cover the oscillatory phenomena in the flow (which do not exceed 200 KHz). Four different sets of data were taken in this fashion, resulting from the

combination of $P_0 = 106$ and 160 psia, and $T_w/T_0 = 0.41$ and 0.8 . At each set data were collected at x -stations separated by an inch, ranging from $x = 29''$ to $x = 44''$.

Figure 1 shows the test model as installed in the wind tunnel while Figure 2 shows the regimes of Reynolds number studied.

4. RESULTS OF THE MEAN FLOW MEASUREMENTS

These are shown on Figures 3 through 5, which present the boundary layer profiles of ρ , T , u and T_t and the boundary layer thicknesses for both laminar and turbulent flow and for the two values of T_w/T_0 chosen. It is seen that for $y > 0.35 \delta$ the data on Figures 3 and 4 settle into profiles which are characteristic of laminar or turbulent boundary layers, depending on Re_x . For $y < 0.35 \delta$, there is obviously probe wall interference and dashed lines are used to indicate the expected trend. Representative theoretical expectations are also shown. Note that fluctuation measurements were reduced at $y/\delta \approx 0.65$, where the laminar state of the flow is clearly defined according to the figures.

Figure 5 presents added evidence of the laminar state of the flow since δ , δ^* and θ are clearly linear functions of the laminar parameter $(x/Re'_e)^{1/2}$. This figure was used to find δ , which is needed to non-dimensionalize stability results to be shortly discussed. For convenience, the boundary layer thickness δ was approximated as follows:

$$\delta = 11.63 \sqrt{\frac{x}{Re'_e}} \quad (\text{inch}) \quad (\text{cold wall}) \quad (1)$$

$$= 14.75 \sqrt{\frac{x}{Re'_e}} \quad (\text{inch}) \quad (\text{hot wall}) \quad (2)$$

Table III shows the key data at each position x where fluctuation measurements were taken.

5. PRINCIPLE OF THE FLUCTUATION MEASUREMENTS

It is implicitly assumed in all experimental work on high speed boundary layer stability (References 2, 3, 6 and 7) that each disturbance mode Q_1 (e.g. velocity fluctuation, temperature fluctuation, etc.), can be written as

$$Q_1 = K \left(x, \frac{y}{\delta} \right) Q_{10} \left(\frac{y}{\delta} \right) \quad (3)$$

provided that the boundary layer is similar, where K is a form of gain and Q_{i0} an initial condition of little concern here. The "gain" K is independent of the type of disturbance. The hot film (or hot wire) anemometer, on the other hand, gives an a.c. response of the type

$$e = \sum_i S_i Q_i = \sum_i S_i \left(\frac{y}{\delta} \right) Q_i \quad (4)$$

where S_i are the sensitivity coefficients. Combining (3) and (4) we get

$$e \left(x; \frac{y}{\delta} \right) = K \left(x; \frac{y}{\delta} \right) \left(\sum_i S_i Q_{i0} \right) \quad (5)$$

and, at constant y/δ ,

$$e(x) = \text{const } K(x) \quad (6)$$

Thus, the hot film response $e(x)$ will be a true indication of disturbance amplification or damping along x regardless of the probe sensitivity or of the way the various modes Q_i participate in making up its a.c. signal.

In the present work, the hot film was traversed continuously across the boundary layer. During tape playback it was possible to choose a given y/δ position at each x and measure the fluctuations there. It was discovered that the maximum in the probe wideband signal occurred always at the same y/δ ($= 0.72$), and it was decided to acquire the data at that position. Thus, for each position listed on Table III, the tape was played at 3-3/4 ips (1/32 the recording speed) and the probe wideband signal was observed; data acquisition began at that point. About 30 feet of tape (equal to an interval of about 0.038) were utilized at each traverse, so, while the data were nominally collected at $y/\delta = 0.72$, they were actually collected in the interval $y/\delta = 0.72 - 0.75$. The TBL-C data, which were replayed in this contract period, were taken at $y/\delta = 0.65$.

6. FLUCTUATION DATA ACQUISITION AND REDUCTION

At each x , acquiring the data consisted of measuring the hot film probe signal spectrum. This was done by a simple system consisting of a wave analyzer and a time-sharing computer terminal (TSS) with a few peripheral pieces of hardware. The wave analyzer was of the digital averaging type; 512 averages at each of 199 Fourier components (frequencies) were taken. After acquisition, each spectrum was converted to digits and stored on cassette. These spectra became the central source of data for the present experiment and for the re-examined fluctuation measurements of Reference 3.

In addition to the probe signals in the boundary layer, electronic noise and freestream turbulence spectra were also recorded.

By combining the spectral density (to the first power) $E(f)$ of each such spectrum (code: SPECXXXX) with the corresponding density $E_n(f)$ of the noise spectrum (code: NOISXXXX) through

$$A(f) \equiv [E^2(f) - E_n^2(f)]^{\frac{1}{2}} \quad (7)$$

one obtains the noise-free square-rooted spectral density $A(f)$ at each frequency f or non-dimensional frequency

$$F \equiv \frac{2\pi f}{u_e Re_e} \quad (8)$$

This is called the amplitude spectrum $A(F)$ at each x or each

$$R \equiv (Re_x)^{\frac{1}{2}} \quad (9)$$

The gain or amplification rate is then defined as

$$G(R, F) \equiv -\alpha_1 \equiv \frac{1}{2A} \frac{\partial A(F, R)}{\partial R} \quad (10)$$

To obtain the derivatives smoothly, the amplitude $A(F; R)$ was first curve-fitted by a fourth degree polynomial as follows:

$$A(R; F) = \sum_0^4 C_1(F) R^i \quad (11)$$

Thus, the amplification rate G , as well as the amplitude A , were found as a function of F and R . The variation $G(F)$ at each R is called the amplification spectrum at that R , while the function $G(R)$ at each F is the amplification change at that F .

The stability diagram is the map of the amplification rate G in the F, R plane. The major purpose of this work is to locate, to the greatest extent and accuracy possible, the major features of stability on this diagram. Such are the neutral branches ($G = 0$ lines) enclosing unstable regions where $G = -\alpha_1 > 0$ (or $\alpha_1 < 0$) and more generally to trace the $G = \text{constant}$ lines. Of special importance are the maximum amplification and maximum damping lines, and the values of the amplification rates along them. The neutral branches can be readily found from the zeros of the amplification change curves (the $R(G=0)$ values at each F) which are printed directly by the STABILIT graphics program on each plot (see Appendix for details of the various programs); as a cross-check, the neutral branches were also found from the zeros of the amplification spectra, i.e. the $G(F)$ plots at each R , which are also plotted by the STABILIT program. Both these methods are employed in the figures

which follow. In the same way, maximum amplification or damping can be found from either the amplification spectra or the amplification change curves, since they both are "cuts" through the stability diagram.

In addition to the above two methods of mapping the stability diagram features (amplification change $G(R)$ at constant F and amplification spectrum $G(F)$ at constant R) the noise-free amplitude spectra $A(F)$ at each R is available in printout form directly from the SPECXXXX files; the amplitude peaks (laminar waves) can be accurately located in frequency from these spectra. Plots of these tables are generated by the PLOTXXXX files.

Another quantity of interest is the absolute magnitude of the Fourier components and their change along the boundary layer. By normalizing each such component $A(F)$ with that measured in the freestream $A_o(F)$ the increase or decrease in $A(F)$ can easily be seen. This scheme then also compares the boundary layer fluctuations with those of the freestream, which are considered to be the source of, and forcing function for, the boundary layer fluctuations (Reference 2). The comparison is thought possible because the probe sensitivity coefficients S_1 (see Equation (4)) do not change much from the stream to the $y/\delta = 0.72$ position in the layer. Accordingly, the freestream spectrum was measured although only for the cases BLT-B, $P_o = 106$ psia, $T_w = 0.8 T_o$ and TBL-C, $P_o = 150$ and 350 psia, $T_w = 0.75 T_o$. This measurement of $A_o(F)$ was done beyond the edge of the layer as far away from the wall as possible, and the most upstream position available for each set of data. The $A(F)$ and $A_o(F)$ were then combined by inputting the PLOTXXXX files into SPECTRO3 program (for printouts of $A(F)/A_o(F)$) or SPECTRO4 for plots. The results are termed the normalized amplitude spectra or the boundary layer response.

The TBL-C results just referred to are the earlier data described in Reference 3 taken with a different model (5 deg. cone) but in the same wind tunnel at $P_o = 150$ and 350 psia and $T_w = 0.75 T_o$. These data were presented in Reference 3 as reduced by older methods which did not allow for the detail and accuracy available with the present data processing software. These older data were, therefore, again processed by the present methods and are shown in this report (designated by TBL-C) in appropriate places.

7. VARIATIONS OF AMPLITUDE AND AMPLIFICATION

Figure 6 shows the variation of amplitude $A(R)$ of a typical Fourier component, with its polynomial curve-fit, while a typical curve of amplification change $G(R)$ is shown on Figure 7. An amplification spectrum $G(F)$ is shown on Figure 8. Curves like those of Figures 6 and 7 were obtained (from the STABILIT program) for each of 199 Fourier components and for each combination of P_o (106 or 160 psia) and T_w/T_o (0.41 or 0.8) and also for the lower-most (BLHF) and the uppermost (FSHF) hot film probe in the rake.

8. STABILITY DIAGRAMS: OVERVIEW

Figures 9 and 10 show the stability diagrams for the cold and hot wall cases as mapped with the aid of data such as shown on Figures 6 to 8. As indicated

by the legend on Figures 9 and 10, most features of the diagrams were redundantly found either by the nodes of the A(R) curves or those of the G(R) curves. The TBL-C data ($T_w/T_o = 0.75$) are compared with the present "hot wall" data; both the earlier version of the TBL-C data (reduced by hand) and the new, computerized reduction of the same data is shown. In the cold wall case (Figure 10) the present data are compared with those of Kendall, although the latter's T_w/T_o (≈ 0.57) is not as low as the cold wall T_w/T_o ($= 0.41$) employed in the present test.

The contents of Figures 9 and 10 will be discussed in more detail in subsequent sections, but are shown at this stage to stress two major points. First, the good consistency of the data is evident. There is agreement between different data-reduction methods, between hot wire (References 2 and 3) and hot film results, between the readings of different probes in the same test when the same model is used in two different wind tunnels and when two different models are used in the same wind tunnel.

Secondly, the complexity of the boundary layer stability at this Mach number is also clear. In both diagrams it is evident that there exist at least three unstable regions ($G = -\alpha_i > 0$), separated by rather narrow stability corridors (regions of damping). The upper bound for the frequencies of unstable oscillations appears to exceed $F = 5 \times 10^{-4}$, while the minimum critical Reynolds number appears to lie below $R = 1100$.

The three unstable regions discerned have been called "lower," "middle" and "upper" and will be commented on immediately below. Amplification rate magnitudes are discussed in Section 12.

9. THE LOWER UNSTABLE REGION

This is shown separately on Figures 11 and 12. The maximum amplification line and the upper neutral branch are very clear, but neither the boundary of the region at low R nor its lower neutral branch have been found.

In the case of the hot wall, (Figure 12) a few maximum amplification points lying below the principal line of maximum amplification seem to define a second such line. From the comments of References 2 and 3, this line evidences the first instability mode, while the principal line of maximum amplification has been identified with waves (with their fronts normal to the flow) belonging to the second instability mode. It is clear, for example, from Figure 13, that the latter mode is then the most unstable phenomenon in this boundary layer. The less important instability, lying below it on Figure 12 and defined by the few available points, is nevertheless a true event, although less conspicuous, as can also be seen from the amplification spectra of Figure 14 for both the hot and the cold wall.

10. THE MIDDLE UNSTABLE REGION

The middle unstable region is plainly visible toward the top of Figures 9 and 10 and are shown separately on Figures 15 and 16. In the case of the cold

wall it is found to contain unstable wavelengths of order 5×10^{-4} in F . Like the lower unstable region, its high Reynolds number extent is detectable by joining the data of References 2 and 3 (especially for the hot walls, Figure 16) to those of the present experiment.

In both cold and hot wall tests, the features of this region (neutral boundaries, etc.), are turning abruptly upward near the lower limit of R investigated; see Figure 15 especially, at $R = 1100$. It seems as if the lower critical R for this region has been reached at such a Reynolds number. Careful scrutiny of the data, however, especially the amplification changes $A(R)$ raise the suspicion that this is a false indication. The reason is that the amplification rate $G(R)$ is the derivative of the curve-fitted polynomial (see discussion in Section 6 and Figures 6 and 7) and it is well known that a curve fit of points within a specific range of a variable is inaccurate at the range end-points. Thus, the points of Figures 15 and 16 that are at or very near $R = 1100, 1370$ and 1650 (the boundaries of the $P_0 = 106$ psia and 160 psia cases studied) should be given less weight.* In view of this the lower neutral branch segment of the middle region at $T_w = 0.41 T_0$, stretching upwards from about $F = 3.5 \times 10^{-4}$ is tentative. Thus, the upper reaches of this middle unstable region do exist but their precise boundaries are provisional.

The instability modes generating this unstable region cannot be fixed. As will be seen below from the amplification rates, the instabilities in this region are certainly more important than those of the first mode. More definite statements must await upon guidance from stability theory (Reference 1).

11. THE UPPER UNSTABLE REGION

Figure 8 illustrates the common observation that, beyond the upper neutral branch of the middle unstable region just discussed, there exists another damping region followed by another unstable region. A small segment of the lower neutral branch of this region can be seen plotted on Figures 9 and 10.

The extent of this region, its contributing modes and its amplification rates cannot be verified from the data reduced so far. However, from the general trend of the data, it is quite certain that its amplification rates are not negligible. Figure 8 leaves a strong impression, in fact, that the amplification spectrum consists of a series of amplification regions possibly extending as high as $F = 10^{-3}$.

*This statement is especially true for the data obtained from the G vs R plots (e.g. Figure 7). The amplification spectra $G(F)$ (e.g. Figure 8) seem to have no such problem.

The effect of cooling the cone model on the "geographic" features of the stability diagram can be seen by comparing Figures 9 and 10. To assist the reader, this comparison is made clearer in Figure 17 where the locus of points of the stability diagrams is replaced by faired-in lines. The effect of cooling is small in that all landmarks are only displaced to slightly larger value of F . The effect on the amplification rates, which will be mentioned below, is considerably larger.

12. THE AMPLIFICATION RATES

The stability diagram (Figures 9, 10, etc.) has so far shown the location of the neutral branches ($G = 0$) and of the maxima/minima of G at constant R or constant F . The magnitudes of these rates are now shown on Figures 18 and 19.

The maximum rates G (or $-\alpha_i$) in the lower unstable region, already identified as due to the second mode $\psi^0 = 0$ waves, are the largest rates at nearly all Reynolds numbers. Toward the smaller Reynolds numbers (the linear regime), the hot-wall maximum rates are nearly constant at about 3×10^{-3} , but they increase to about 5×10^{-3} when $T_w/T_0 = 0.41$ (Figure 18). The first mode instabilities are much less potent with their G being of order 1×10^{-3} under the same conditions. No clean-cut change of these latter instabilities has been discerned when T_w/T_0 changes (Figure 14).

The middle-region amplification rates (Figure 19) are surprisingly large; in the linear regime they are only slightly smaller than those of the lower region. These instabilities can, therefore, by no means be discounted as having a decisive influence in the boundary layer destabilization and transition to turbulence.

13. MAXIMUM AMPLITUDE LAMINAR WAVES

The passage of Fourier components through the lower unstable region generates the intense "laminar waves" recorded photographically in Reference 3. The locus of frequency F variation with R is shown on Figures 13, 20 and 21 for these waves (denoted as the "maximum amplitude" line) and its proximity to the maximum amplification line leaves no doubt that these waves are connected with the $\psi^0 = 0$ waves of the second mode, as already suggested in Reference 2. The maximum amplitude line is so inclined in the F - R diagram so that the wave frequency shifts to lower values as one moves downstream along the cone (with increasing R). This well-known shift is illustrated by the amplitude spectra $A(f)$ of Figure 20. The maximum amplification line of the middle unstable region generates a corresponding peak in the amplitude spectra at a frequency nearly twice that of the "primary" laminar waves; this "second harmonic" can be clearly seen in the amplitude spectra, e.g. Figures 13 and 20.

The new element introduced by the present data is the measurement of the peak frequency of these waves in the entire range $1100 < R < 2400$, which in turn shows its interesting variation relative to the maximum amplification

line and upper neutral branch (Figure 21). At low R the waves are most prominent near the maximum amplification line but farther downstream, the maximum amplitude line approaches and crosses the upper neutral branch, near $R = 1700$; thereafter the laminar wave peak in the spectra decreases. The maximum in the peak intensity coincides with the onset of increases in the high frequency components of the spectrum, and the "randomization" of the spectrum, as already documented in Reference 3, i.e., the beginning of transition. What is presently unknown is whether transition is the cause or the result of the loss of strength of the laminar waves.

The wavelength of the laminar waves was computed from

$$\frac{\lambda}{\delta} = \frac{u_e}{f\delta}$$

where the layer thickness δ was obtained from the laminar boundary layer measurements (see Figure 5). The results, seen on Figure 22, show that $\lambda \approx 2\delta$, with a slight increase in λ/δ caused by downstream distance or wall cooling.

14. FREESTREAM INPUTS AND THE BOUNDARY LAYER RESPONSE

The effect of the freestream disturbances on the fluctuation amplitudes and amplification rates can be gathered from Figures 23 through 25. The former effect is mainly of interest to the transition problem, since it can shed light on the total amplification needed to cause transition. The second effect has a bearing on the distortion of the stability characteristics in the presence of finite input disturbances (Mack's "forcing" theory, see Reference 2). Records of the freestream disturbances existed in three sets of the present series of data: the TBL-C 350 psia data set, the 150 psia set of the same experiment and the present (BLT-B) test at 106 psia and hot wall ($T_w = 0.8T_0$).

In his study of the same problem (which he calls "the boundary layer response"), Kendall utilized the freestream spectrum as recorded ahead of the test model in supersonic flow. In the present case, the freestream measurements were done just above the model surface at the x position where the first fluctuating boundary layer data of each set were taken.* This was done partly of necessity and partly because it was felt that the true input "seen" by the layer lies within the shock cone and not upstream of the model. (This point may be in error, as will be seen below). The response of the boundary layer is the fluctuation spectrum $A(f)/A_0(f)$ where $A_0(f)$ is the freestream disturbance input (i.e., the spectral density, to the first power, at f). At lower M_∞ , Kendall was able to demonstrate that the boundary layer response at representative R was as expected from theory (Reference 1).

*For example, in a set of data covering from x_1 to x_2 at $y/\delta = 0.72$, the freestream turbulence was measured at x_1 and $y/\delta \approx 3$.

In the present work the three sets of reduced data, if viewed individually and notwithstanding the unavailability of companion theoretical results, show a response performance which is close to intuitive expectations. Figure 23 shows that for the TBL-C $P_0 = 150$ psia data the laminar wave instability is absent at $x = 19''$ ($R = 1166$) but appears and grows at subsequent positions. The datum at $R = 1166$ is especially important since, by the fact that $A/A_0 = 1$ across the spectrum, it implies a completely inert boundary layer upstream of this Reynolds number. This contradicts Kendall's finding that the freestream disturbances enter the layer near the apex of the body and grow monotonically thereafter.

Figures 24 and 25 show the last-in-line datum from the $P_0 = 150$ psia series ($R = 1628$, Figure 24) and the first-in-line datum from the 350 psia series ($R = 1780$, Figure 25) of the TBL-C test. If the response A/A_0 is only a function of R , then these two sets should be "joining" smoothly, i.e., the spectrum of Figure 24 should not differ much from the spectrum of Figure 25. It can be seen that this is not the case and that the response at $R = 1780$ is abruptly larger than that at $R = 1628$. Furthermore, this jump from the one set of data to the other cannot be due to $A_0(f)$ since the freestream spectra are quite similar (Figure 26). Thus the jump is due to the numerator $A(f)$ of the response A/A_0 . We then conclude that, although the freestream spectrum changed hardly at all, the amplitude content at fixed R is larger for the larger P_0 (or unit Reynolds number). One explanation, by no means unique, is that the amplification rates are different in the region $R < 1000$ (because they are found similar at $1000 < R < 1800$) when the tunnel unit Reynolds number changes.

Adding to the confusion is the observation that for the new (BLT-B) tests, the response at $P_0 = 106$ psia looks, in the region $1100 < R < 1500$, just like that for TBL-C, $P_0 = 350$ psia in the region $1500 < R < 2000$. To indicate this graphically, note the maximum amplitude (of the laminar waves) taken from figures such as 24, 25, etc., and plotted on Figure 27. Other than an obscure trend of a maximum $A/A_0 \approx 30$ for the laminar waves, there is no way the three independent sets of data can be rationalized.

Finally, it must be stressed that the quantitative comparison of amplitudes is always subject to errors arising from the interpretation of the hot wire or hot film probe signal. The transfer function linking fluctuation amplitudes to the probe signal varies from one probe to another and depends on tunnel pressure, on the particular fluctuation mode active, and on frequency. It is, therefore, felt that with theoretical results not yet available and with the question of probe signal interpretation still open, no further discussion of the boundary layer response is justified here.

15. THE NON-LINEAR REGIME AND TRANSITION TO TURBULENCE

The results presented in the preceding sections have been discussed with frequent reference to hydrodynamic stability theory, which is a (linearized) small disturbance theory. Yet, in the range $1500 < R < 2500$ the fluctuations

measured in this work are large (in Reference 3 describing the TBL-C tests the resolved wideband fluctuations are of order 20-30%). In the regime of transition to turbulence ($R > 2300$ for $T_w/T_o = 0.8$), the laminar wave intensity actually decreases by spectral dispersion; in the sense of the stability diagram this dispersion is coincident with the laminar wave maximum amplitude line crossing the upper neutral branch of the lower unstable region (see Figure 21).

In viewing the stability diagram (Figures 9, 10, etc.), it would be very desirable to draw demarkation boundaries marking regimes where the disturbance level is low enough to be compatible with linear stability theory. However, no theoretical guidelines exist on what a "small" disturbance precisely is.

The most striking feature of the stability diagram is its smoothness, without discontinuities or abrupt changes in behavior, through the non-linear, transitional and turbulent regimes; this is especially evident in the "hot wall" case ($T_w = 0.8 T_o$).

Thus, the concepts of disturbance amplification, damping, etc., are apparently valid over a range much wider than hitherto thought. In this connection, the "stable corridor" between the lower and middle unstable regions assumes a new significance in the transitional regime. This "corridor" now contains the laminar waves, and in the turbulent flow the spectrum peak due to these waves must decay. Thus, in the transitional regime, the laminar wave decay (spectral dispersion) is embodied in this corridor of damping. Furthermore, in the turbulent boundary layer, the fluctuation levels are self-similar, by definition, along constant y/δ lines. Thus, all amplification (or damping) rates must eventually become zero toward the right hand margin of the stability diagram. Consequently, the turbulent boundary layer limit of the stability diagram must consist of a large neutral region, as opposed to neutral "branches" found in the upstream, "linear" regime. The decay of the amplification rates towards neutrality ($G \equiv -\alpha_1 = 0$) can already be seen in Figures 18 and 19.*

In the present experiment, transition in the cold wall case was found to occur roughly between $Re_x = 3.3 \times 10^6$ and 4.3×10^6 , as opposed to about 5×10^6 for the hot wall case. The amplification rates for the cold wall case are also about double those of the hot wall case (cf Figure 18). Here is, therefore, first evidence that disturbance amplification and transition to turbulence are consistent, since transition moves upstream when the amplification rates (in both the lower and middle unstable regions) increase.

At this Mach number, both Reference 3 and the present work agree that transition is caused by dispersion of the laminar waves, both in the spectrum and

*In the transition zone, the boundary layer profile loses similarity; thus the rationale of keeping the sensor at constant y/δ , described in Section 5, is no longer valid. Some numerical adjustment, probably quite small, is thus needed for all data at large R ($R > 2000$) shown here.

the energy sense. It is reasonable to propose, furthermore, that the boundary layer will be most vulnerable to turbulence breakdown when the laminar waves attain their maximum amplitude, which occurs when their maximum amplitude line crosses the upper neutral branch (of the lower unstable region) as shown on Figure 21. This is reinforced by a careful scrutiny of this figure, which shows that the crossing occurs earlier ($R \approx 1500$) in the cold wall case than in the hot wall case ($R \approx 1800$). Thus, the "crossing" Reynolds number Re_x ($\sim R^2$) is about 40% lower in the case of the cold wall, or a percentage about equal to the decrease of the transition Reynolds number in the cold wall case, as mentioned above.

A tentative picture of the transition mechanism at this Mach number, as viewed from the standpoint of laminar stability, is as follows: the most unstable region in the boundary layer is the lower unstable region in which second-mode waves with $\psi = 0$ and $-\gamma_1$ of order 5×10^{-3} generate laminar waves. By the time these waves exit the unstable region they have grown to the point where they can cause laminar breakdown. The effect of cooling is to displace both the neutral branch and the maximum amplitude line so that the two cross at a smaller Reynolds number, thus causing a proportional decrease in the transition Reynolds number.

This proposal answers a question posed earlier in this report by stating that the crossing of these two lines is the cause, not the result, of transition; if valid it would be equally so for Mack's "forced" theory. The question then arises whether transition could not be predicted by computing the locus of the maximum-amplitude line and the upper neutral branch, which is undoubtedly in the realm of the non-linear stability problem.

16. SUMMARIZING DISCUSSION AND CONCLUSIONS

Major results of this study, presented in this summary only briefly, are as follows:

16.1. The results obtained in this experiment are consistent with all other data reported to date at $M_\infty \approx 7$. A complete picture of disturbance amplification is thus available at this M_∞ in the range $1100 < R < 2400$ (or $1.2 \times 10^6 < Re_x < 5.8 \times 10^6$) and for T_w/T_0 down to 0.4. Moreover, the consistency of the results of three independent experiments done with essentially different wind tunnels and models, removes suspicion that the instability was grossly influenced by peculiarities of the flow or the test article.

16.2. The present results fully vindicate the admonition of Mack and others that boundary layer stability at hypersonic speeds is a complex phenomenon. No fewer than three distinct unstable regions have been found in contrast to the single instability "loop" encountered at subsonic or supersonic speeds. Unstable disturbances exist for $F > 4 \times 10^{-4}$, or considerably higher in frequency than previously thought.

16.3. The boundaries and amplification rate isotherms have been isolated with considerable precision. The "lower unstable region" has been mapped over the

entire range of $1100 < R < 2400$. A lower neutral branch for this region has been tentatively identified but its minimum Reynolds number has not been found. By inference from the work of Mack, this region is the one generated by inclined first mode, and normal second mode instabilities. It is clear that the first mode, which dominates instabilities at lower Mach numbers, is rather unimportant.

16.4. The middle unstable region, newly mapped in this work, serves to amplify disturbances at considerably higher frequencies than the first region. What is surprising about this region is its rather large amplification rates; these are nearly the same as those found in the lower unstable region, i.e., of order 2 to 5×10^{-3} . Precisely what instability mode is active here is presently unknown.

16.5. A third unstable region (here called "upper unstable") also exists. Information of this region is still fragmentary, but it must involve wavelengths of order 0.26 or smaller.

16.6. The passage of each Fourier component through the unstable regions results in the formation of the well-known "laminar waves." Of these, the prominent ones belong to the lower unstable region (and to the second instability mode) while the growth of a weaker "second harmonic" has also been observed, associated with the middle unstable region. Physically, the waves are about twice as long as the boundary layer is thick. The significant feature of these waves is the new finding that the locus of their maximum amplitude on the stability diagram eventually crosses the upper neutral branch of the lower instability region. By the definition of the neutral branch, this crossing signals the end of the growing period of the laminar waves and the onset of boundary layer transition.

16.7. The act of lowering the surface temperature from 0.8 to 0.4 has only a negligible effect on the location and size of the unstable regions and a similarly slight effect on the laminar waves, but the amplification rates nearly double in both the lower and the middle unstable regions. This overall increased rate of amplification could only mean earlier transition to turbulence, exactly as observed. This marks the first occasion where the cooling effects on amplification and transition were recorded simultaneously; their mutually consistent behavior should renew confidence in the relevance of hydrodynamic stability to the boundary layer transition problem.

17. THE NEED FOR ADDITIONAL DATA

The following extensions of the present experiments are recommended:

1. Mapping of the stability diagram at this Mach number ($M = 7$) in the same R range but higher frequencies ($F > 5 \times 10^{-4}$), to discover the highest frequencies capable of amplification. Also, mapping is needed at all frequencies but at $R < 1100$ to discover the minimum R , if any, at which disturbances amplify.

2. A more thorough investigation of low frequency signals ($F < 10^{-4}$) at the present R range ($1100 < R < 2300$) to discover the lower neutral branch of the lower unstable region.

3. A more thorough search for a connection between the freestream disturbance spectrum and the content of the boundary layer, including freestream turbulence measurements ahead of the model.

In addition to these experiments, it will be extremely important to have theoretical calculations available, such as linear stability theory computations of the amplification rates $G \equiv -\alpha_i$ as a function of F and R. It will be equally important to identify the instability modes generating the middle and upper instability regions found by the present measurements. Quantitative estimates of the effect of cooling would be put to good use by comparing them with the increased amplification rates due to cooling observed in this test; in fact, any quantitative small disturbance theory (including Mack's "forcing theory") would be useful. Finally, the fact that the stability diagram transits smoothly across the regimes of linearity, non-linearity and transition should be an inducement for theorists to approach the non-linear problem.

TABLE I

HOT FILM PROBE CHARACTERISTICS
AND OPERATING CONDITIONS

Probe type: Hot film anemometer

Physical Characteristics: Probe body: 0.02" dia. Kimax glass rod
(wedge shaped at tip)

Film material: platinum

Film dimensions: 0.002" x 0.02"

Leads: gold

Probe Number: FO-4

Film room resistance: 150.7 ohm

Equilibrium resistance in flow: 238 ohm (typical)

Operating characteristics: $i = 9.833 \text{ ma}$ (fixed)

Overheat: 10%

Amplifier: ADP 1213 (VKF)

Gain: 50

Electronic compensation: 500 microseconds

Amplifier set bandwidth: $0.05 \text{ KHz} < f < 500 \text{ KHz}$

TABLE II

OVERALL EXPERIMENTAL CONDITIONS

Wind tunnel: AEDC/B

Mach No. freestream: $M_{\infty} = 8.0$

Supply temperature: 1310°R

Supply pressure: 106, 160 psia (fluctuations only)

Stream Reynolds No.: 40,500 per inch (106 psia)

61,120 per inch (160 psia)

Model: 4-deg. half-angle right circular cone

Surface: smooth, impermeable

Bluntness: zero

Angle of attack: zero

Surface temperature: 537°R , 1048°R

Boundary layer edge conditions (typical):

Edge velocity: 3,770 fps = 1,150 m/sec

$Re_e = 42,100$ per inch = 16,600 per cm (106 psia)

= 63,550 per inch = 25,020 per cm (160 psia)

TABLE III
DATA LIST

$T_w = 0.41 T_o$			$(u_e)_{ave} = 3765 \text{ fps} = 45180 \text{ ips}$			
$P_o = 106 \text{ psia}$		$(Re')_{ave} = 4.212 \times 10^4 \text{ in}^{-1}$		Code 21XX, $F=0.33 \times 10^{-8} f$		
Group No.	X(inch)	Tape	Footage	$\delta(\text{inch})$	$\sqrt{Re_x}$	$u_e/f\delta$
39	Noise	202	1043			
40	29	202	1194	0.305	1105	2.19
41	30	202	2910	0.31	1124	2.26
42	31	202	3893	0.315	1143	2.23
43	32	202	5977	0.32	1161	2.29
44	33	202	7089	0.325	1179	2.16
45	34	203	287	0.33	1198	2.21
46	35	203	2210	0.335	1214	2.27
47	36	203	3193	0.34	1231	2.2
48	37	203	5539	0.345	1248	2.17
49	38	203	7122	0.349	1265	2.16
50	39	204	0	0.354	1282	2.27
51	40	204	1807	0.359	1298	2.30
52	41	204	3619	0.363	1314	2.35
53	42	204	5359	0.368	1330	2.31
54	43	204	7197	0.371	1346	2.26
55	44	205	0	0.376	1361	2.26

			$(u_e)_{ave} = 3781 = 45368 \text{ ips}$			
$P_o = 160 \text{ psia}$		$(Re')_{ave} = 62.2 \times 10^3 \text{ in}^{-1}$		Code 22XX, $F=0.223 \times 10^{-8} f$		
Group No.	X(inch)	Tape	Footage	$\delta(\text{inch})$	$\sqrt{Re_x}$	$u_e/f\delta$
37	29	201	3846	.251	1343	2.22
36	30	201	2981	.255	1366	2.26
35	31	201	2047	.260	1389	2.31
34	32	201	1070	.264	1411	2.27
33	33	201	0	.268	1433	2.26
32	34	200	7172	.272	1454	2.28
22	35	199	6333	.276	1475	2.31
23	36	199	7399	.280	1496	2.24
24	37	200	0	.284	1517	2.26
25	38	200	839	.287	1537	2.34
26	39	200	1764	.291	1557	2.34
27	40	200	2587	.295	1577	2.36
28	41	200	3426	.299	1597	2.48
29	42	200	4308	.302	1616	2.44
30	43	200	5237	.306	1635	2.49
31	44	200	6169	.309	1654	2.58
14	Noise	199	1081	-	-	-
15	Noise	199	1239	-	-	-

TABLE III
(Continued)

$T_w = 0.8$		$(u_e)_{ave} = 44940 \text{ ips}$				
$P_o = 106 \text{ psia}$		$(Re')_{ave} = 42.12 \times 10^3 \text{ in}^{-1}$		Code 11XX,	$F=0.331 \times 10^{-8} f$	
Group No.	X (inch)	Tape	Footage	δ (inch)	$\sqrt{Re_x}$	$u_e/f\delta$
61	29	205	1770	.387	1105	1.9
63	30	205	6577	.394	1124	1.89
64	31	206	0	.4	1143	1.91
65	32	206	1715	.407	1161	2.02
67	33	206	3750	.413	1179	1.92
68	34	206	5552	.419	1197	1.96
69	35	206	7242	.425	1214	1.95
70	36	207	0	.431	1231	1.94
71	37	207	1635	.437	1248	1.91
72	38	207	3900	.443	1265	1.94
73	39	207	5801	.449	1282	1.89
75	40	208	0	.454	1298	1.97
76	41	208	1847	.46	1314	1.96
77	42	208	3861	.466	1330	1.87
78	43	208	5416	.471	1346	2.05
79	44	208	6941	.476	1361	1.99
66	Noise	206	3528			

$P_o = 160 \text{ psia}$		$(Re')_{ave} = 62.2 \times 10^3 \text{ in}^{-1}$		$u_e = 45204 \text{ ips}$		
				Code 12XX,	$F=0.223 \times 10^{-8} f$	
81	44	209	0	.392	1654	2.05
82	42	209	1910	.383	1616	2.01
83	40	209	3756	.374	1577	2.03
85	38	209	5272	.365	1537	2
86	36	209	6870	.355	1496	2.03
87	34	201	5486	.345	1454	2.01
88	32	201	7510	.335	1411	1.95

TABLE III
(Continued)

$$T_w = 0.8 T_o$$

$$(Re'_e)_{ave} = 4.212 \times 10^4 \text{ in}^{-1}$$

$$F = 0.331 \times 10^{-8} f$$

Code 55XX
Exterior (FSHF) Probe

Group No.	X (inch)	Tape	Start Footage	δ (inch)	R	$u_e/f\delta$
61	29	205	1770 (or 5070)	-	-	-
66	Noise	206	3528	-	-	-
63	30	205	6577	.394	1124	
64	31	206	0	.4	1143	
65	32	206	1715	.407	1161	
69	35	206	7242	.425	1214	
70	36	207	0	.431	1231	
71	37	207	1635	.437	1248	
72	38	207	3900	.443	1265	
73	39	207	5801	.449	1282	
75	40	208	0	.454	.298	
76	41	208	1847	.46	1314	
77	42	208	3861	.466	1330	
78	43	208	5416	.471	1346	
79	44	208	6941	.476	1361	
61	29	205	1770	.387	1105	

TABLE III
(Continued)

TBLC DATA
 $P_o = 350$ psia $T_w/T_o = 0.75$ Tape 65
Code 24XX $u_e = 44881$ ips
 $F = 0.838 \times 10^{-9} f$

X(inch)	Footage	Counter Freq.	δ (inch)	$Re_x \times 10^6$	$R = \sqrt{Re_x}$
F.S.	1504	-	-	-	-
Noise	6751	-	-	-	-
19	1179	.045	.134	3.17	1780
21	1808	.103	.147	3.51	1873
23	2242	.166	.155	3.84	1960
25	2682	.226	.161	4.18	2045
27	3151	.287	.168	4.51	2124
29	3529	.348	.177	4.84	2200
31	3950	.407	.18	5.18	2276
33	4484	.465	.186	5.51	2347
35	5097	.523	.192	5.85	2418
37	5597	.578	.197	6.17	2483
39	6240	.634	.202	6.51	2551

$P_o = 150$ psia Code 23XX $F = 0.195 \times 10^{-8} f$

F.S.	7551	-	-	-	-
Noise	6751	-	-	-	-
19	7239	.039	.205	1.36	1166
23	7721	.161	.237	1.65	1285
25	8052	.225	.246	1.79	1338
27	8462	.286	.257	1.93	1389
31	8869	.408	.275	2.22	1490
33	9352	.466	.284	2.36	1536
35	9891	.526	.293	2.50	1581
37	10434	.584	.301	2.65	1628

REFERENCES

1. Mack, L.M., "Linear Stability Theory and the Problem of Supersonic Boundary Layer Transition," AIAA J., Vol. 13, No. 3, March 1975, pp. 278-289.
2. Kendall, Jr., J.M., "Wind Tunnel Experiments Relating to Supersonic and Hypersonic Boundary Layer Transition," AIAA J., Vol. 13, No. 3, March 1975, pp. 290-299.
3. Demetriades, A., "Boundary Layer Instability Observations at Mach Number 7," J. of App. Mech., ASME, Vol. 99, No. 1, pp. 7-10, March 1977.
4. Donaldson, J.C., "Measurements in a Study of Laminar Boundary Layer Stability on a 4-Degree Sharp Cone at Mach Number 8," Rept. AEDC-DR-77-62, ARO Inc., Arnold AFS, Tenn., 19 July 1977.
5. Laderman, A.J., "Review of Wind Tunnel Freestream Pressure Fluctuations," AIAA J. Vol. 15, No. 4, April 1977, pp. 605-608.
6. Demetriades, A., "An Experiment on the Stability of Hypersonic Laminar Boundary Layers," JFM Vol. 7, Part 3, March 1960, p. 385.
7. Laufer, J. and Vrebalovich, T., "Stability and Transition of a Supersonic Laminar Boundary Layer on an Insulated Flat Plate," J. Fl. Mech., Vol. 9, Part 2, October 1960, pp. 257-299.

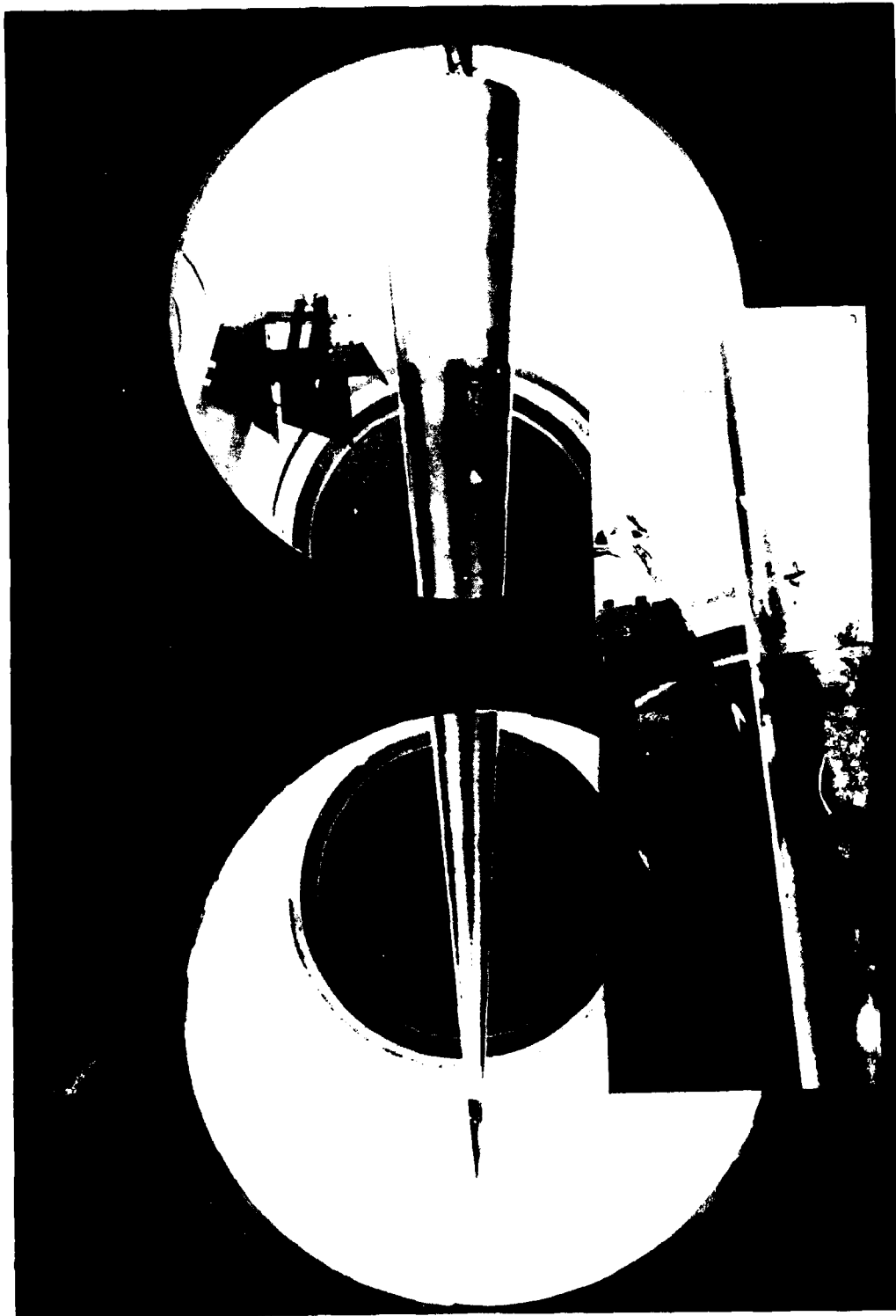


Figure 1. Cone model installation in the wind tunnel. Inset shows hot film probe close to the surface with second probe positioned higher to sample simultaneously the freestream turbulence (pitot tube and total temperature probe are not clearly visible).

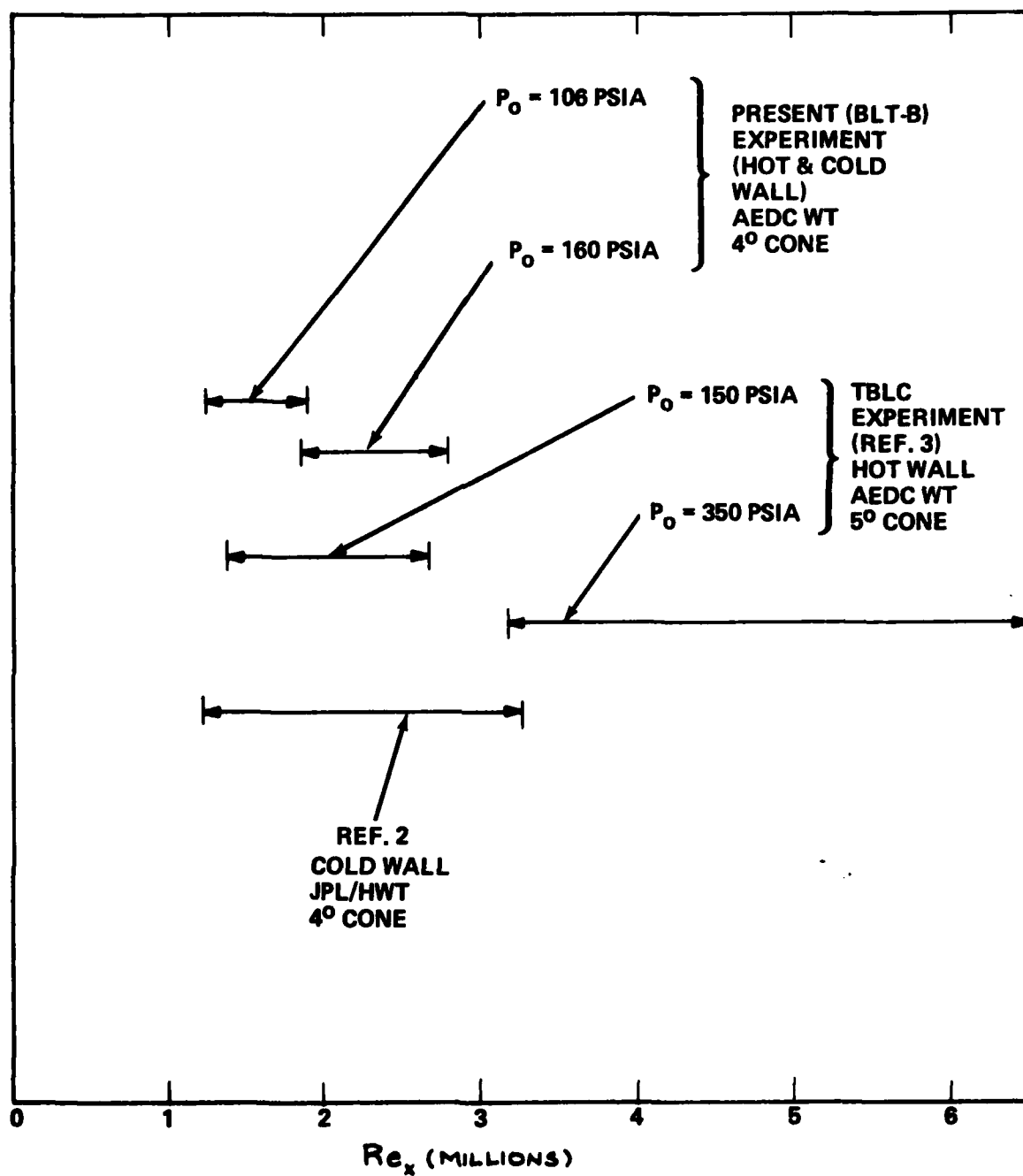


Figure 2. Reynolds number ranges investigated.

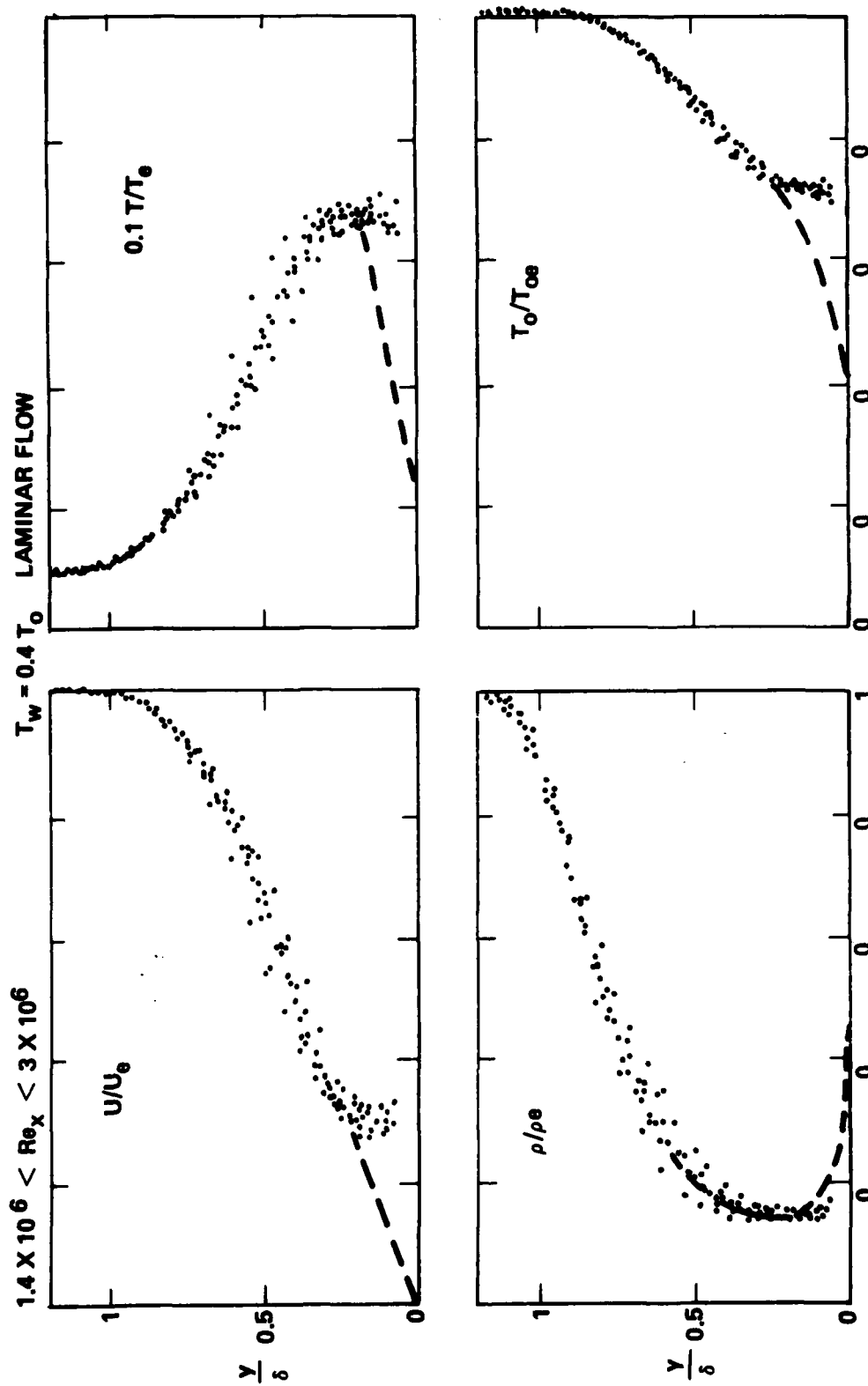


Figure 3. Measured boundary layer profiles with cold wall, laminar flow. Dashed lines represent expected variations near the wall.

27

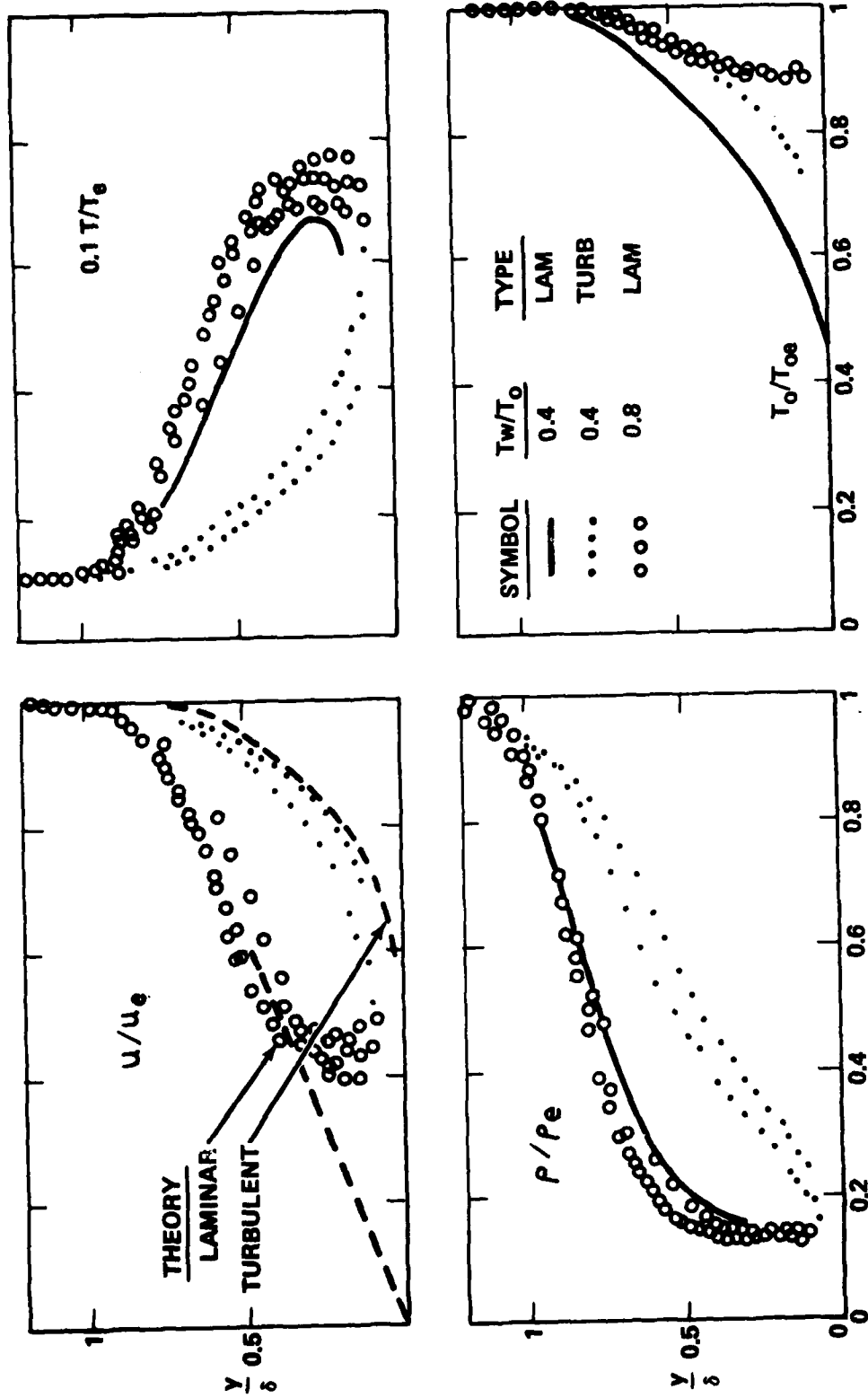


Figure 4. Laminar and turbulent profiles for both cold and hot wall.

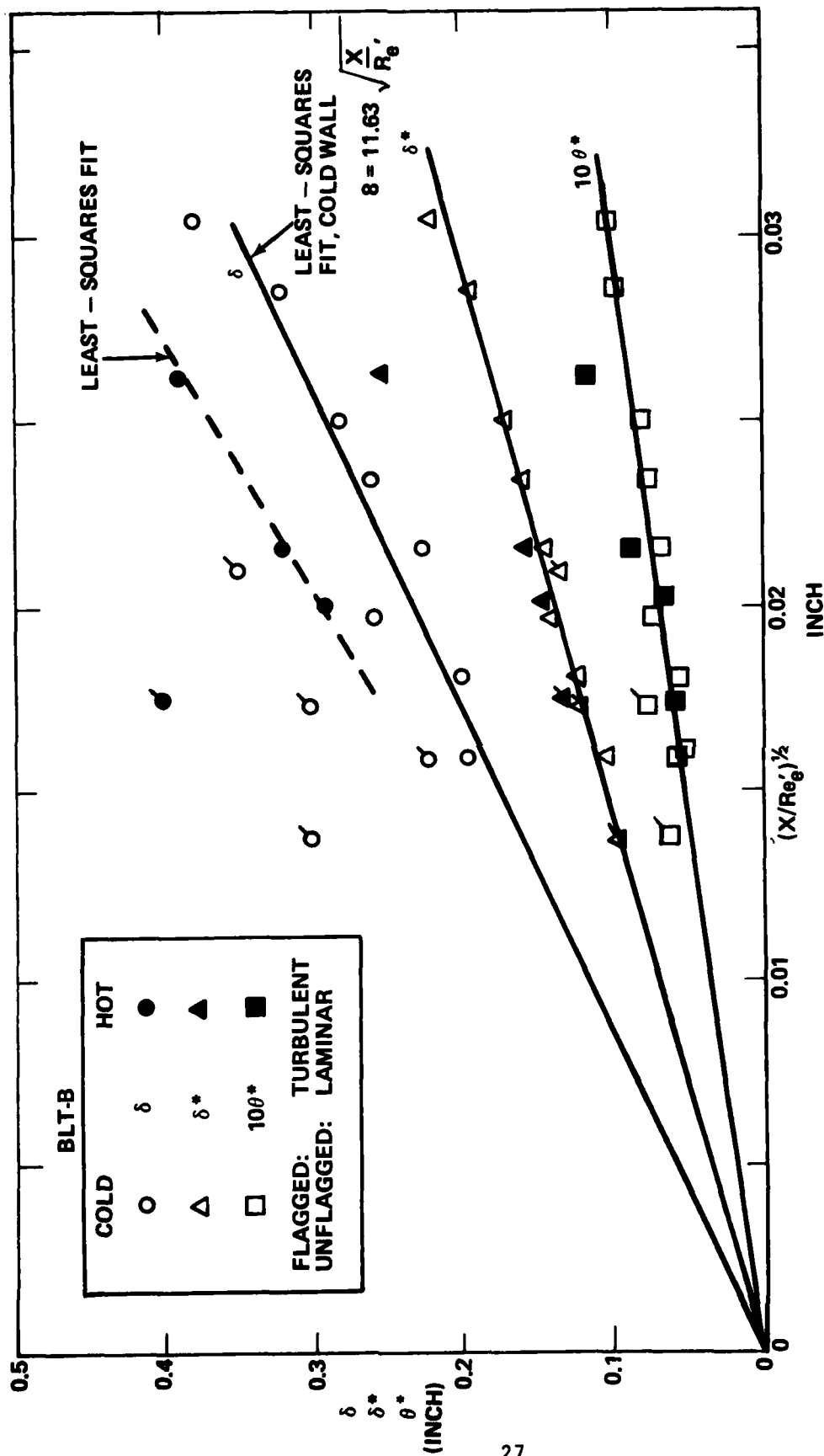


Figure 5. Measured boundary layer thicknesses.

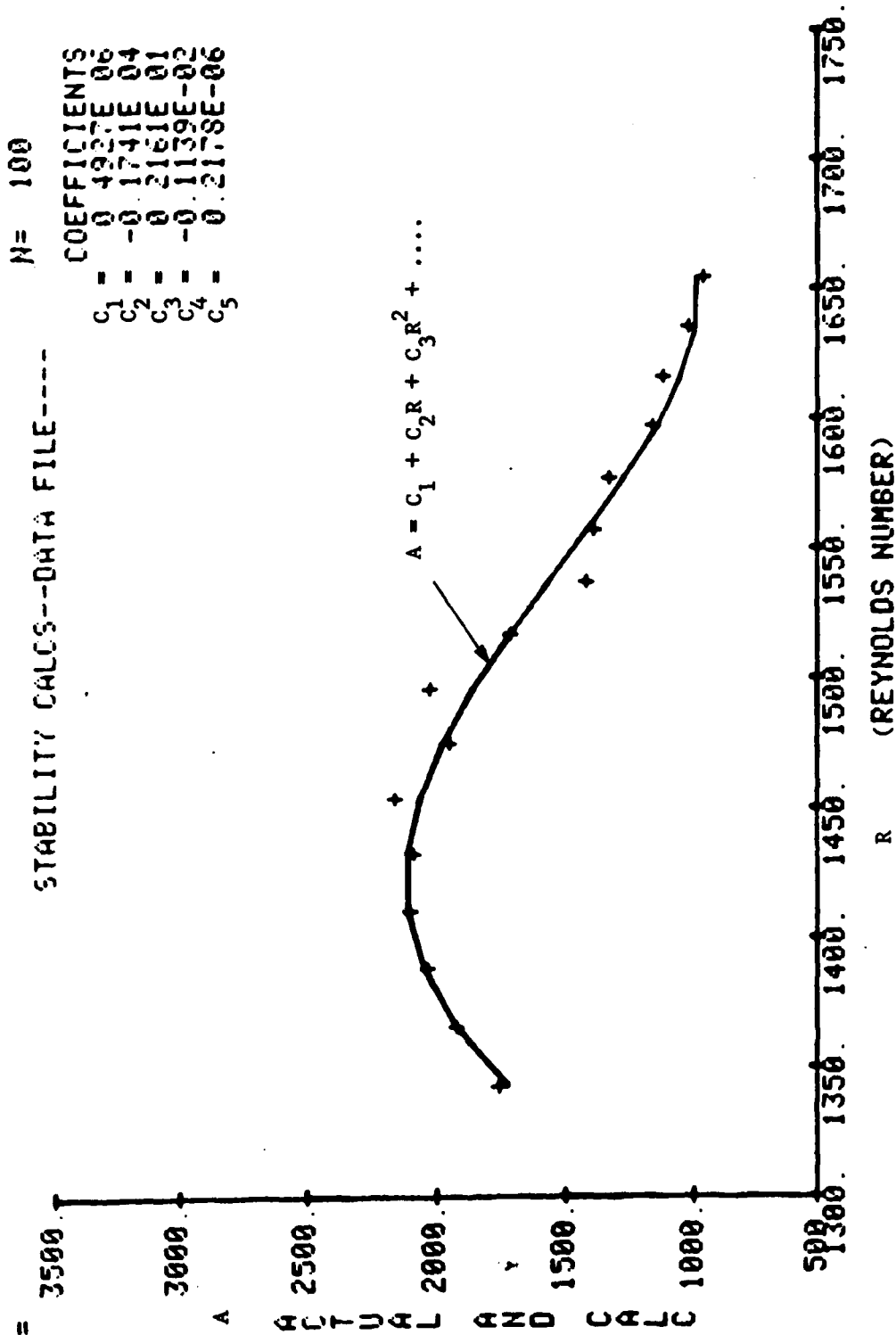


Figure 6. Typical variation of a Fourier component (in this case $N = 100$ signifies 80 KHz) along the cone surface at $y/\delta = 0.72$. Data (crosses) are least-squares curve fitted by solid line. In this example, an upper neutral branch (entry of the waves into a damped region) occurs at about $R = 1420$.

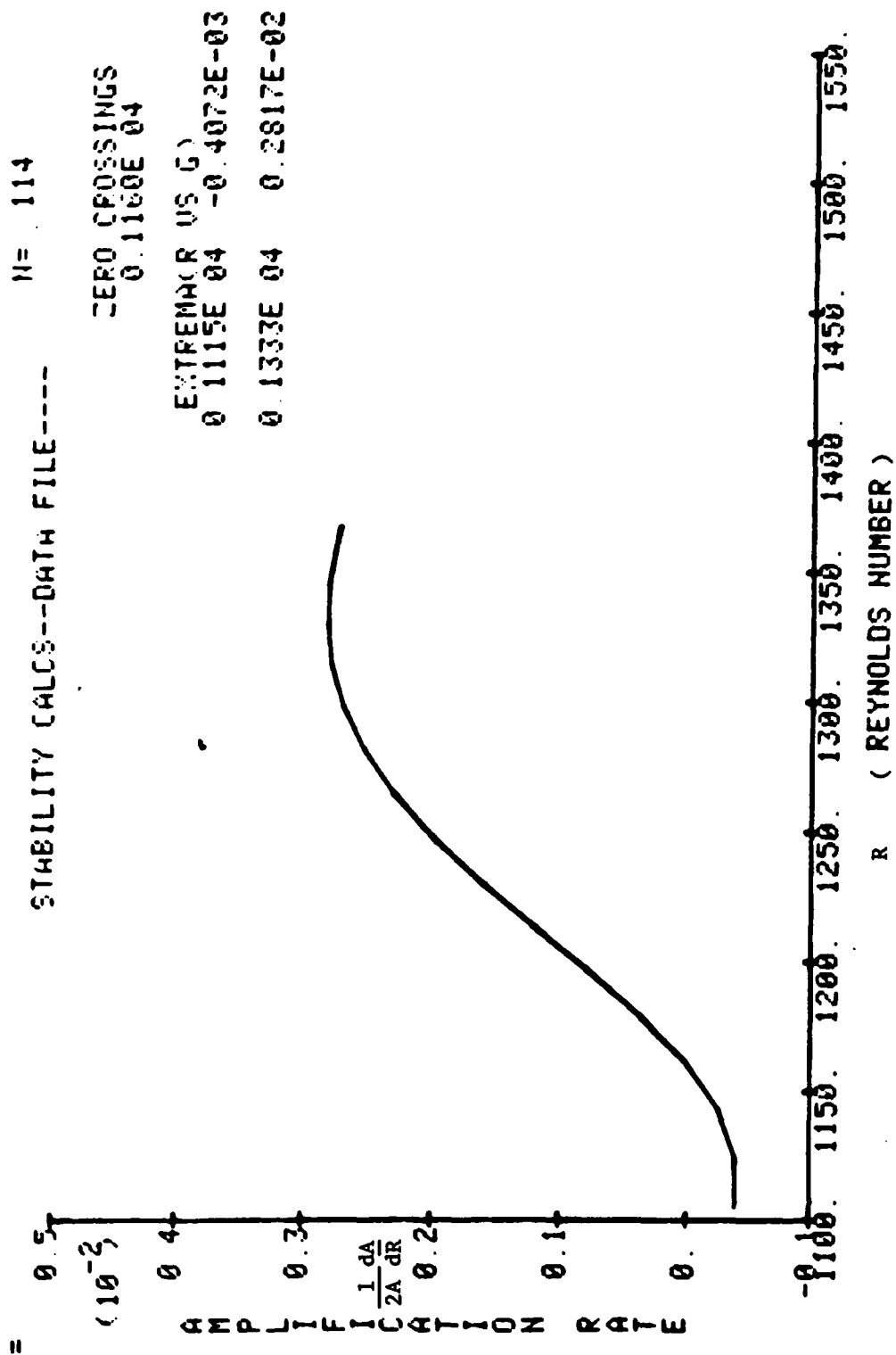


Figure 7. Typical variation of amplification rate with Reynolds number. Note how the computer automatically provides the neutral branch location at R = 1160 (in this case a lower branch) and the coordinates of maximum damping (at R = 1115, $-\alpha_1 = -0.000407$) and maximum amplification (at R = 1333, $-\alpha_1 = 0.00282$).

DATA FILE----- P= 1597.0000

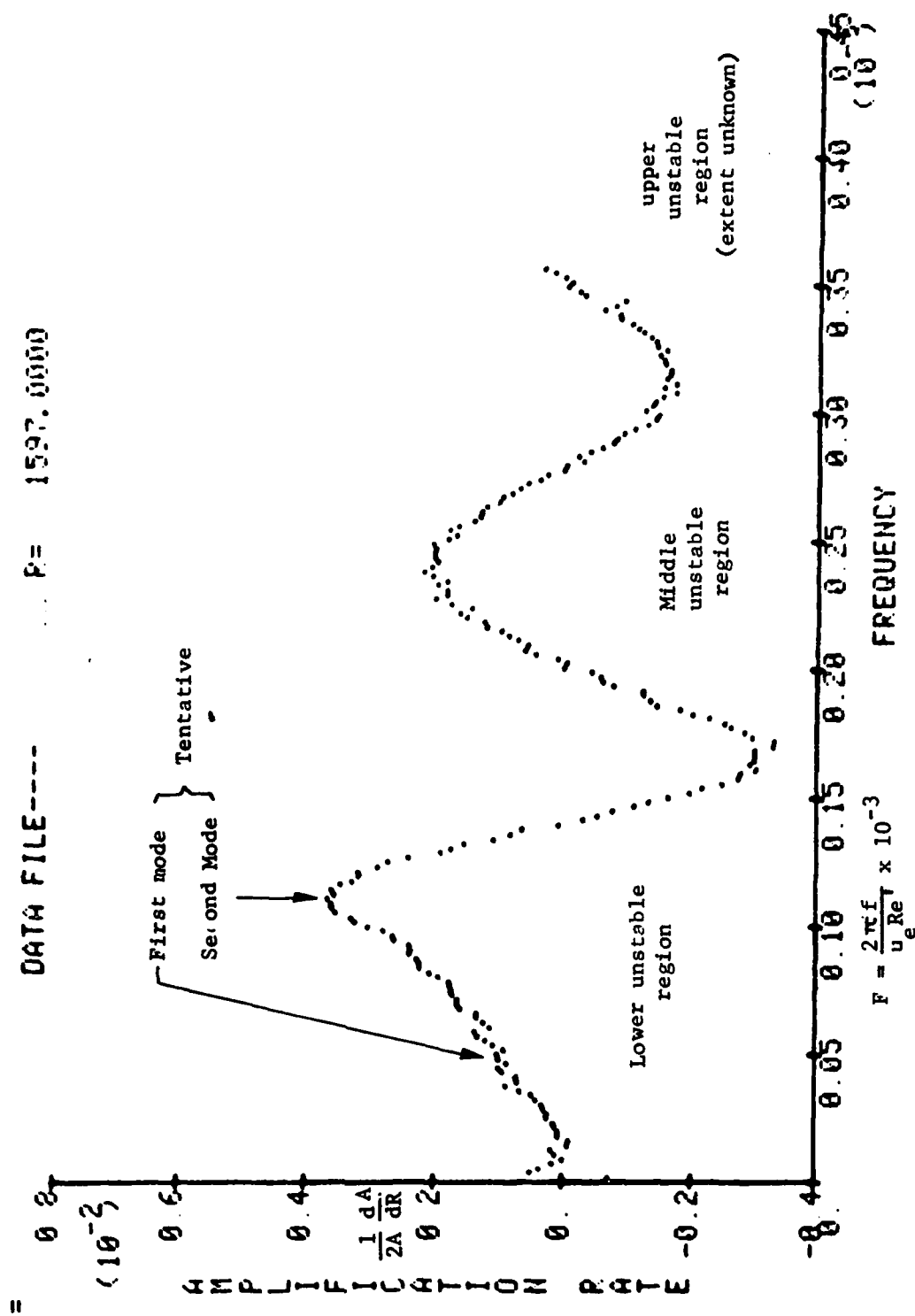


Figure 8. Typical amplification rate spectrum, in this case for supply pressure of 160 psia, $T_w = 0.41 T_o$ and $R = 1597$ ($Re_x = 2.55 \times 10^6$). Earlier studies dealt with the left hand half of this spectrum. The middle and upper unstable regions were found in the present experiment.

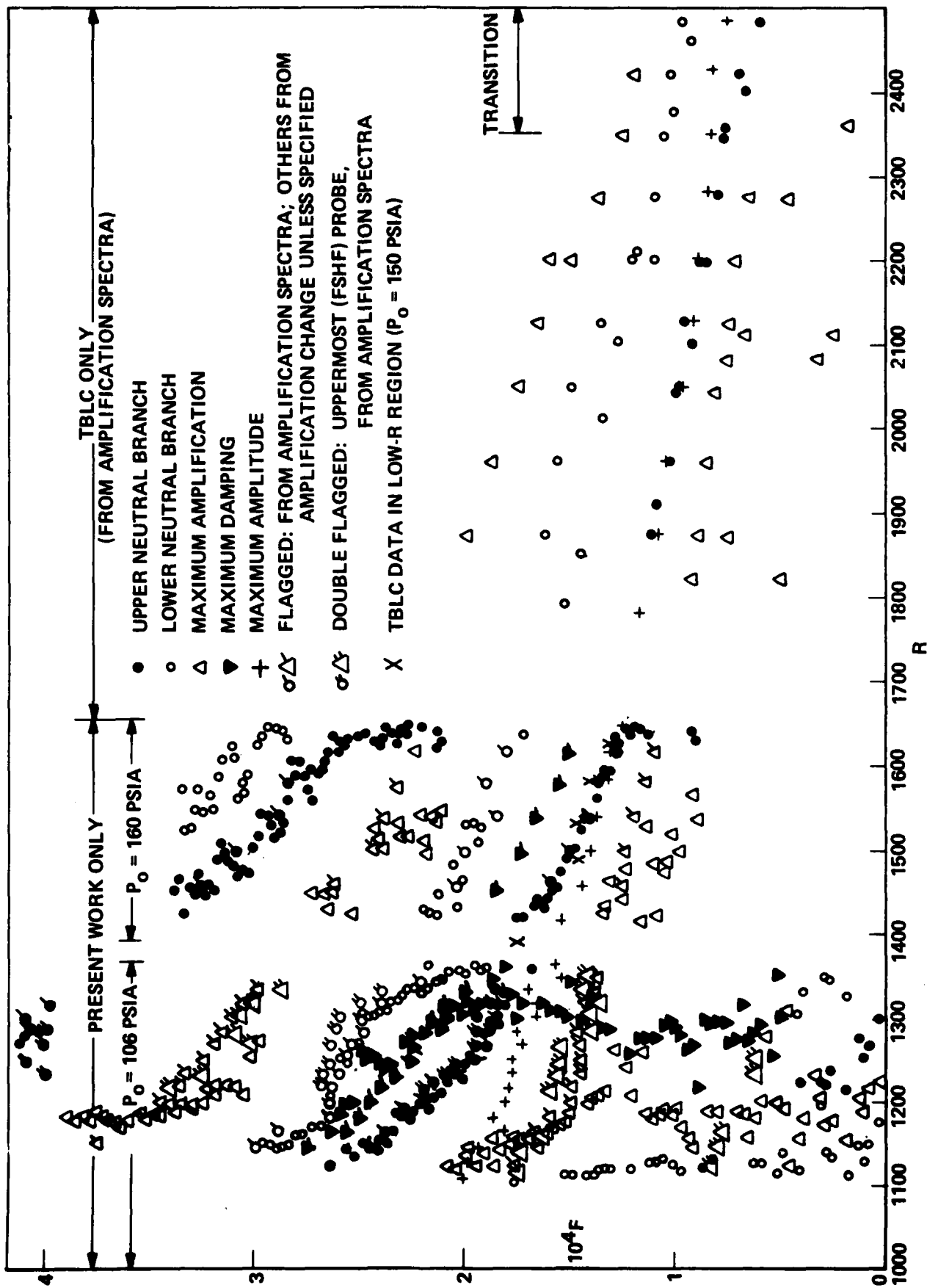


Figure 9. Experimental results on the overall stability diagram with $T_w/T_0 = 0.8$.

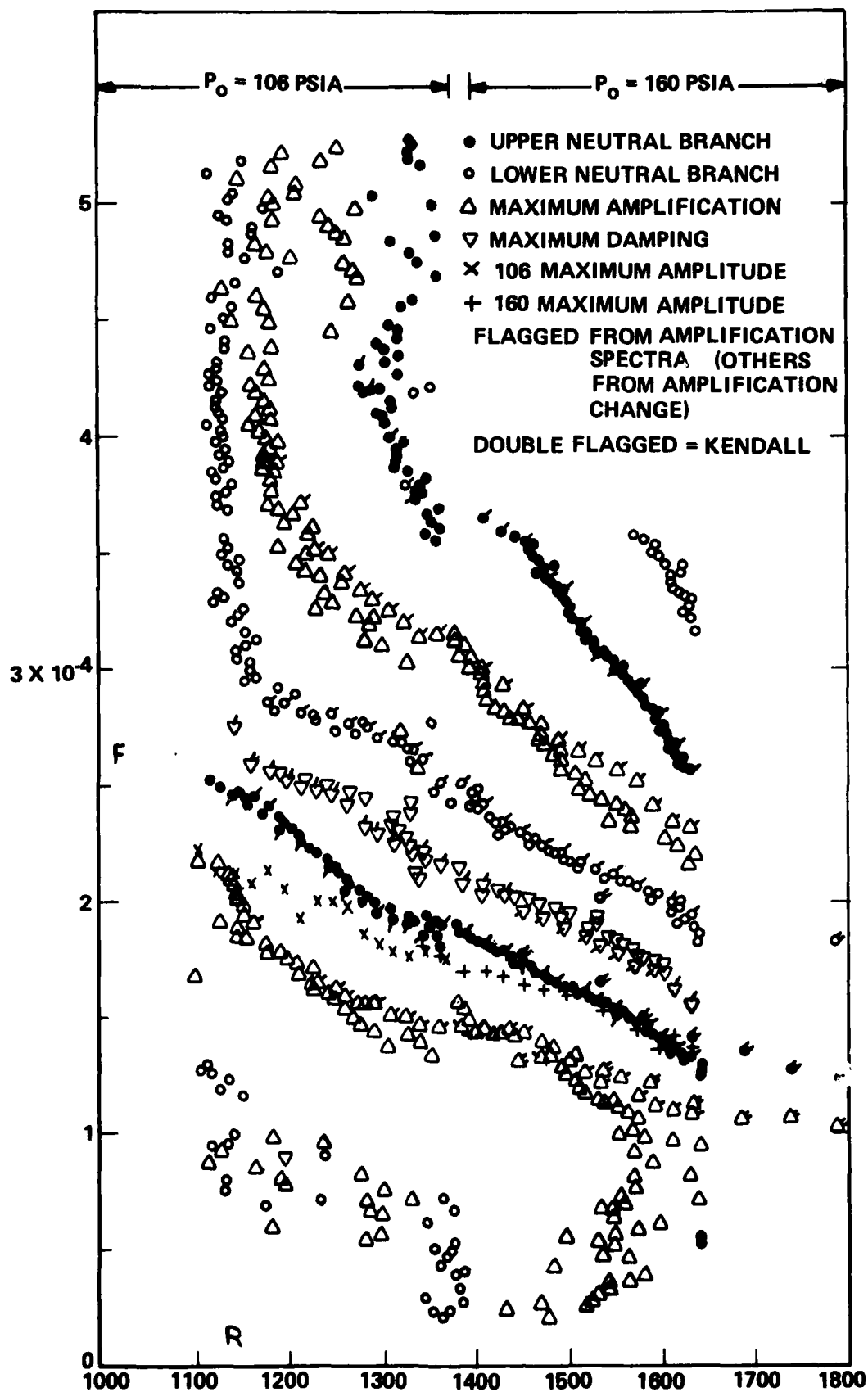


Figure 10. Experimental results on the overall stability diagram with $T_w/T_0 = 0.41$.

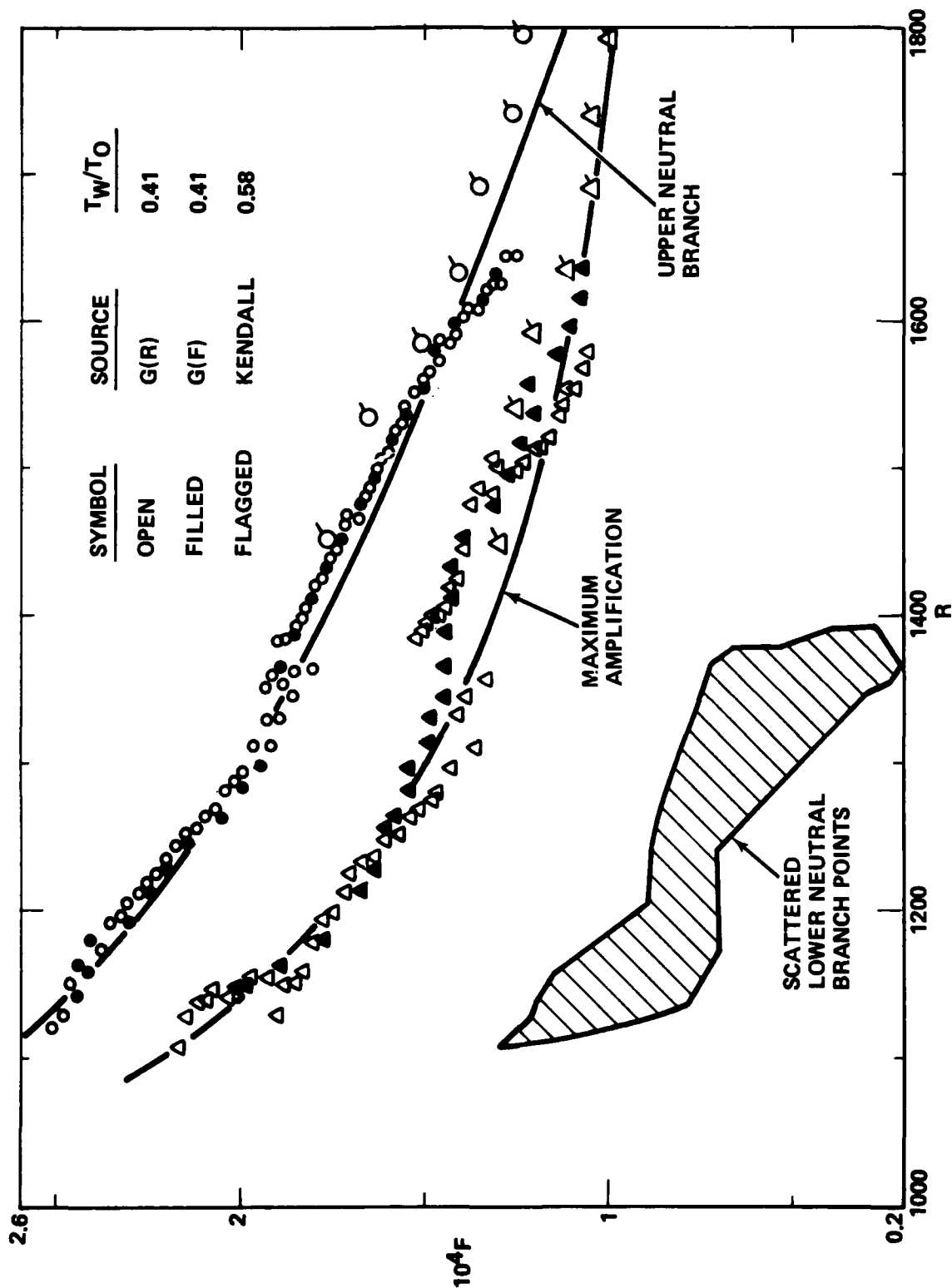


Figure 11. Experimental results on the lower unstable region in the cold wall case.

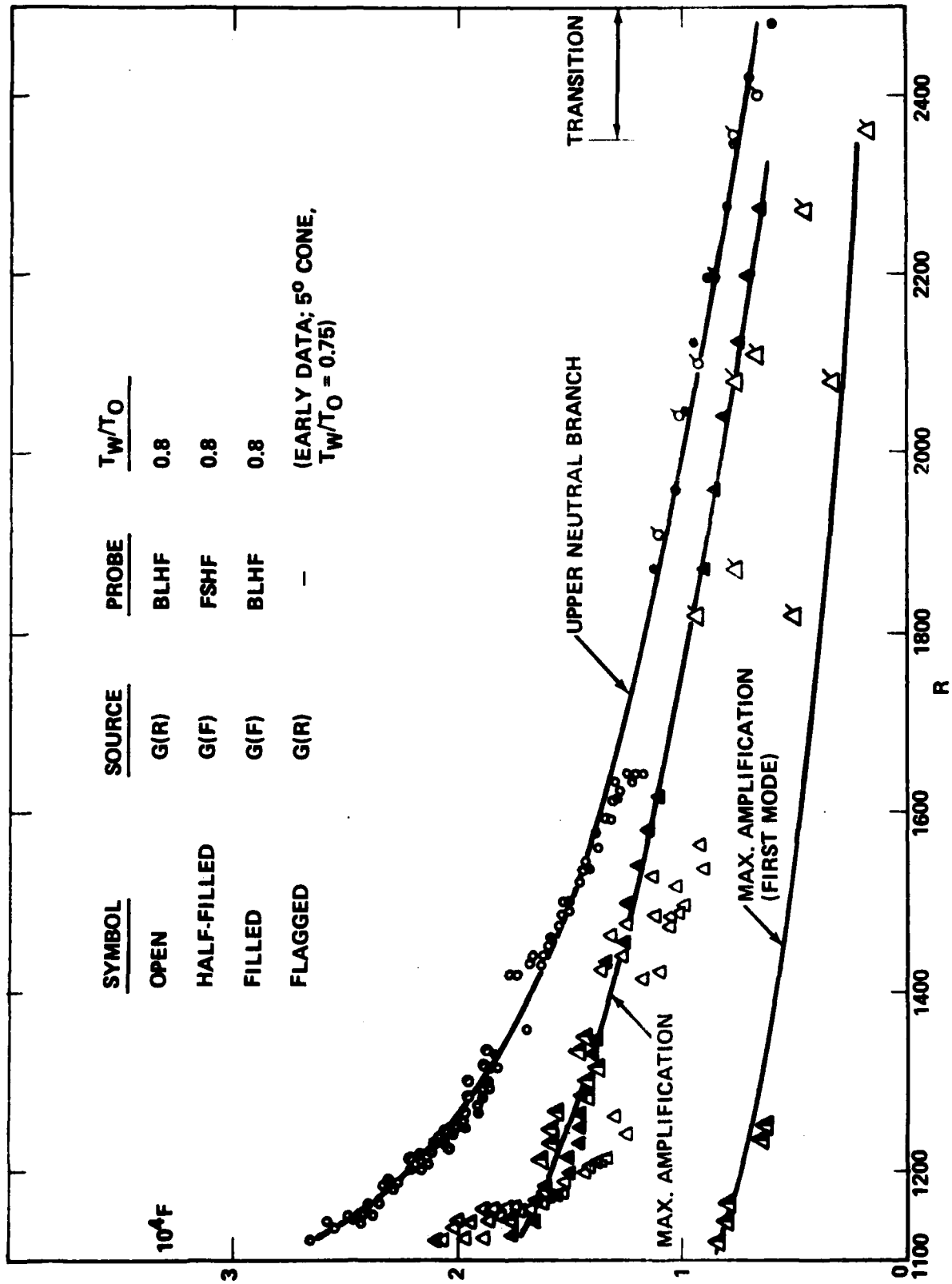


Figure 12. Experimental results on the low unstable region hot wall case.

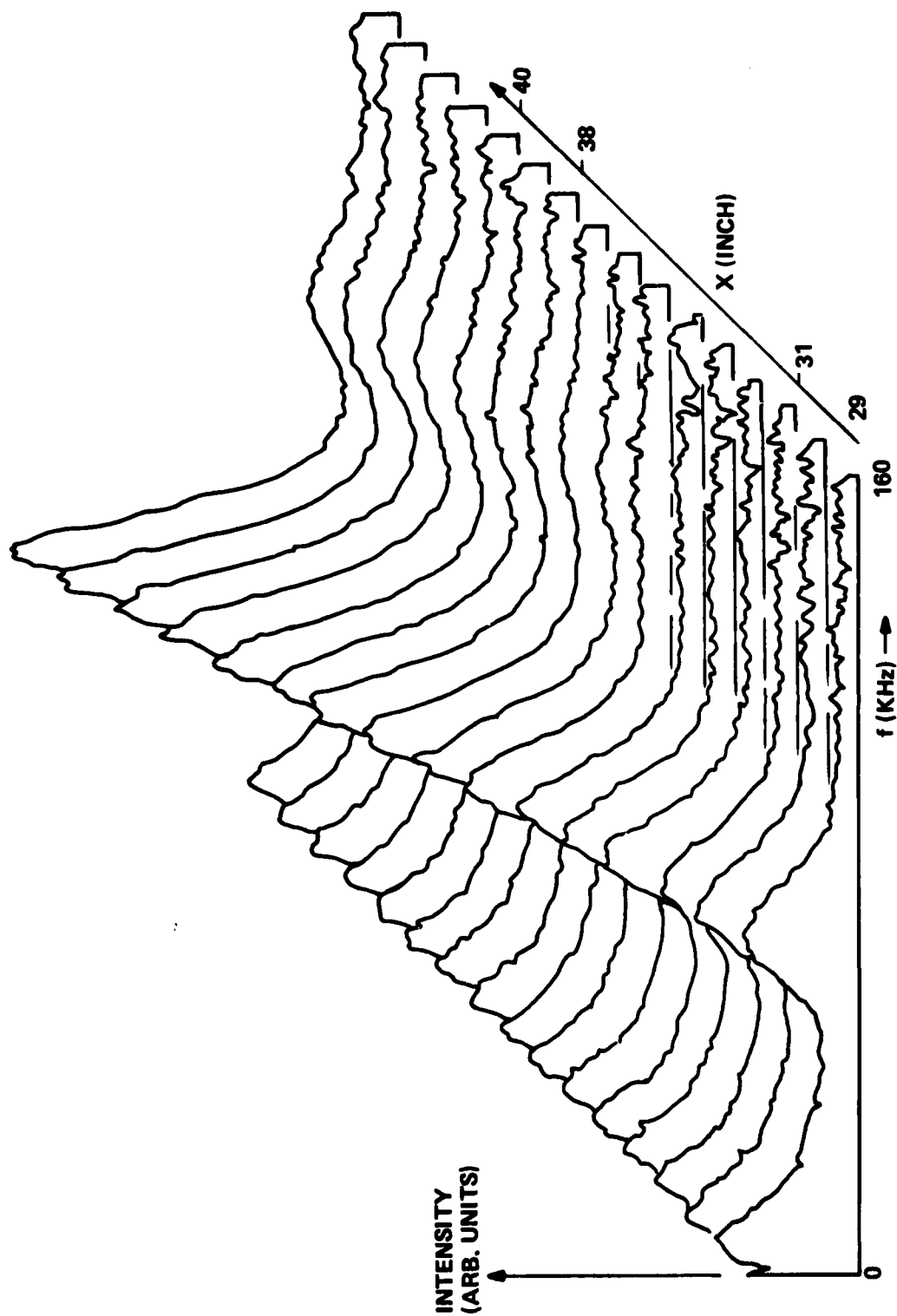


Figure 13. Fluctuation spectra at $y/\delta = 0.72$, supply pressure of 106 psia and $T_w = 0.41 T_o$. Note the growth of the laminar waves and the emergence of the second harmonic as one proceeds downstream.

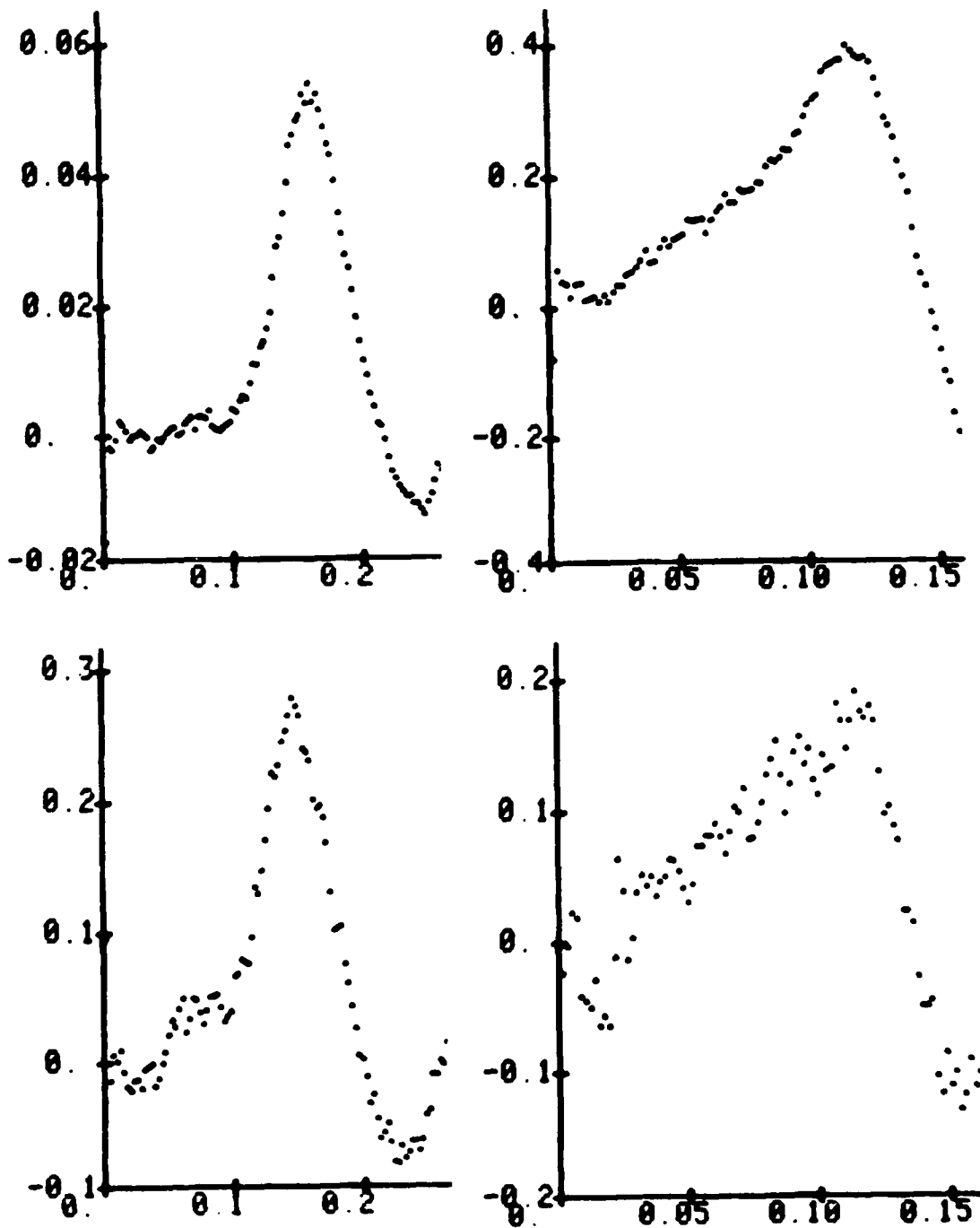


Figure 14. Evolution of the amplification spectra $G(F) = -\alpha_1(F)$ for the cold (above) and hot (below) wall cases. Spectra at left are for $R = 1248$, those at right at $R = 1577$. First instability mode is thought to lie between the prominent peak and the ordinate axis.

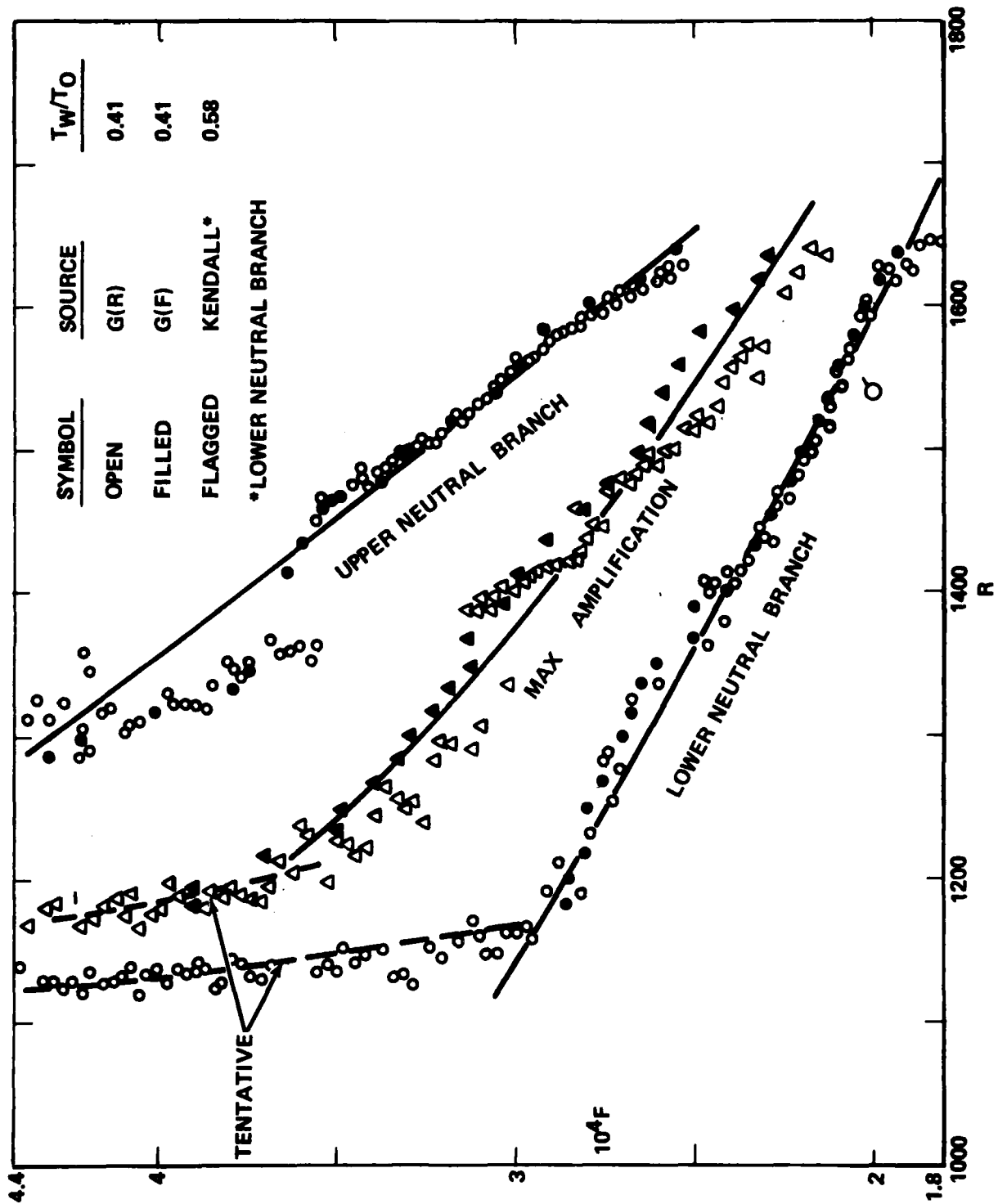


Figure 15. Experimental results on the middle unstable region, cold wall case.

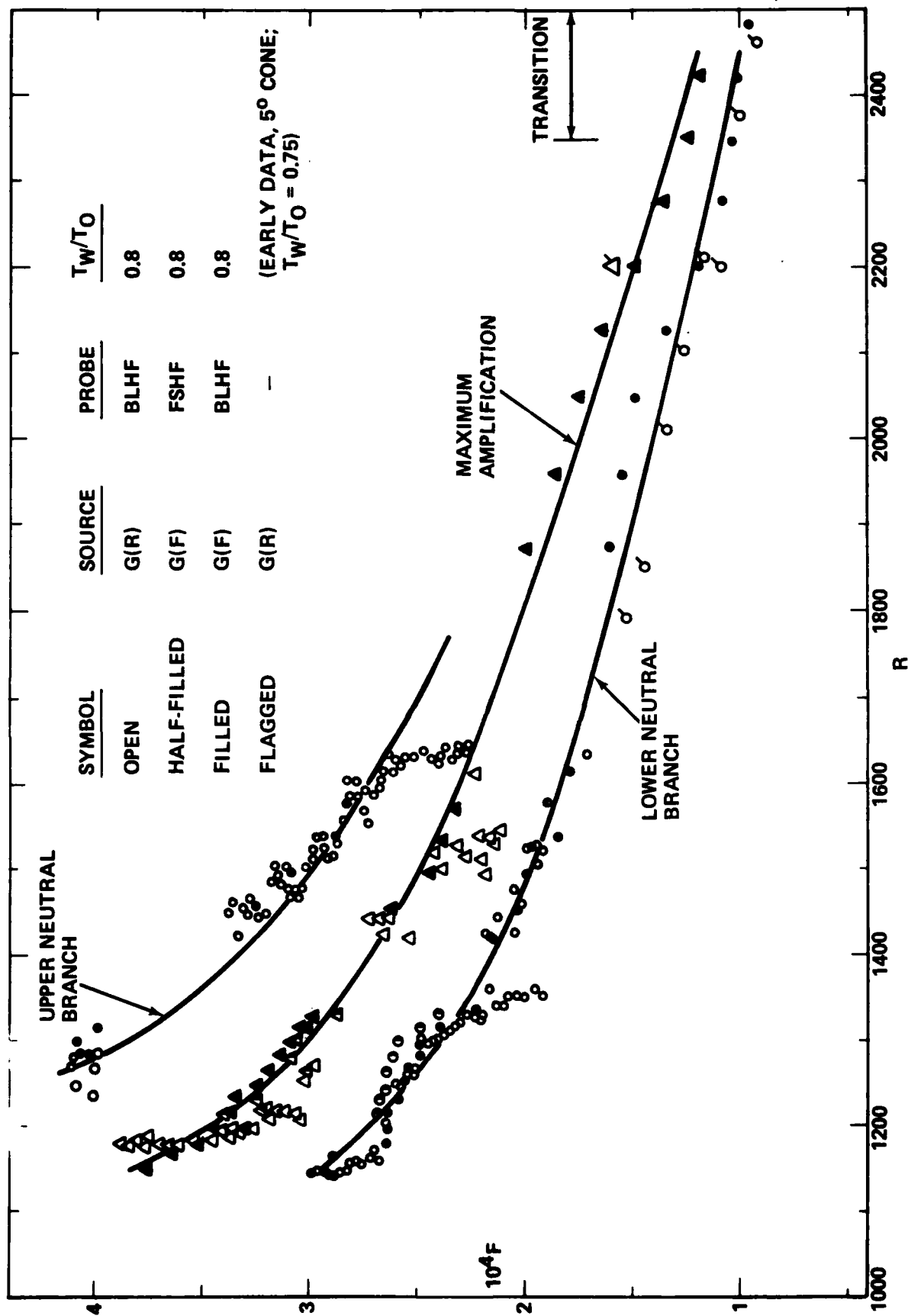


Figure 16. Experimental results on the middle unstable region, hot wall case.

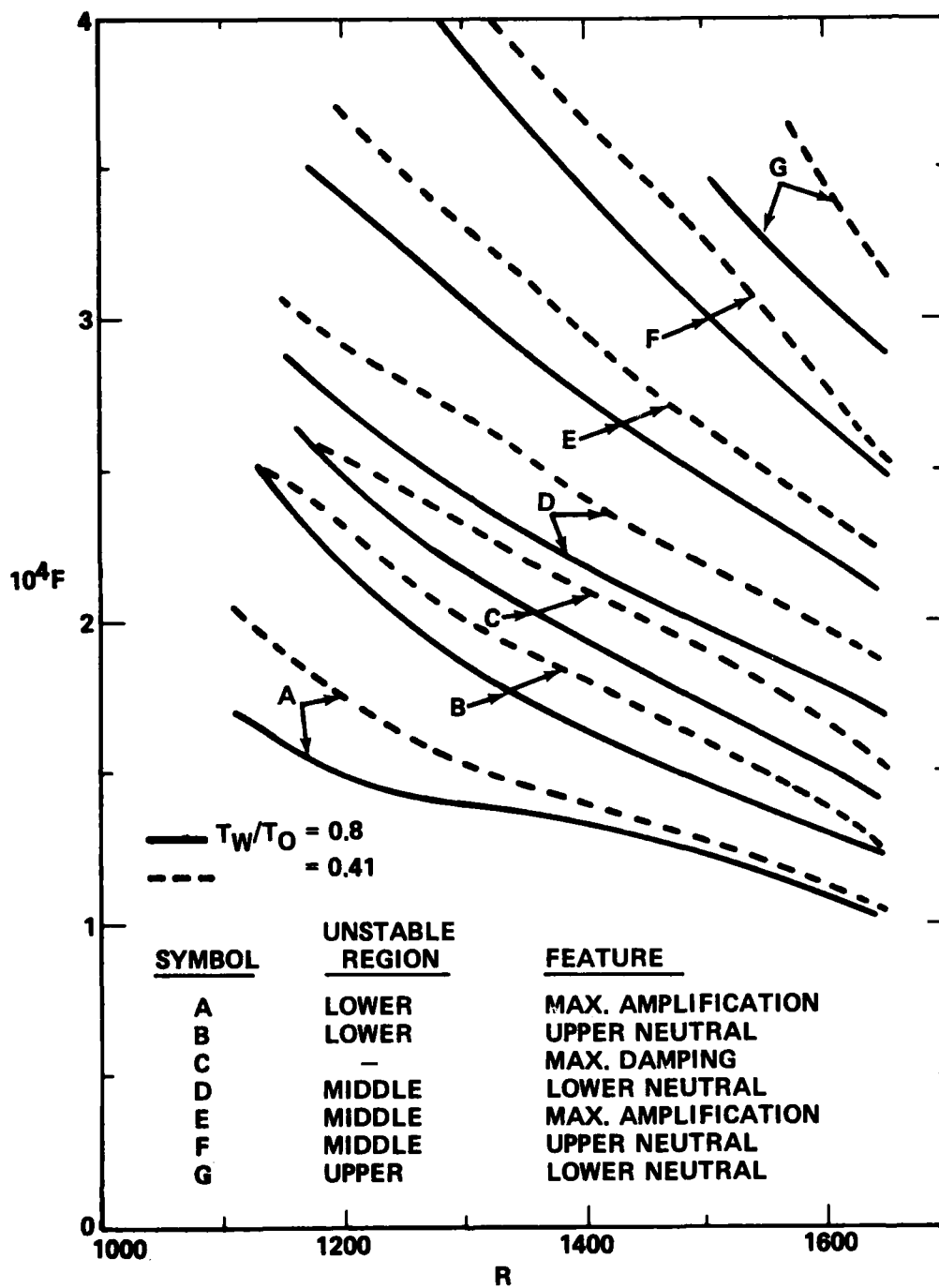


Figure 17. Effect of wall temperature on the major features of the stability diagram.

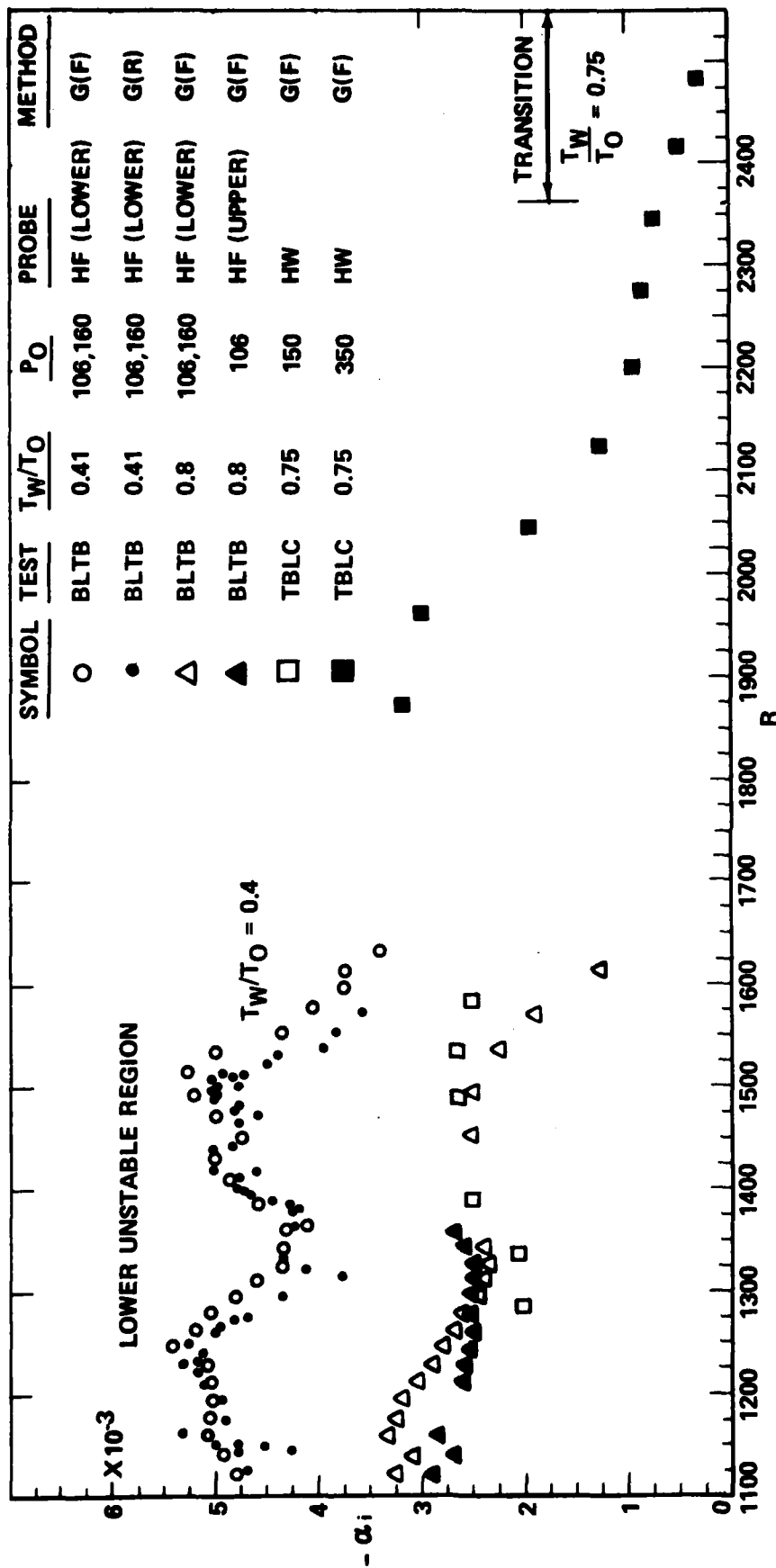


Figure 18. Maximum amplification rates in the lower unstable region (second mode instabilities, $\psi_0 = 0$).

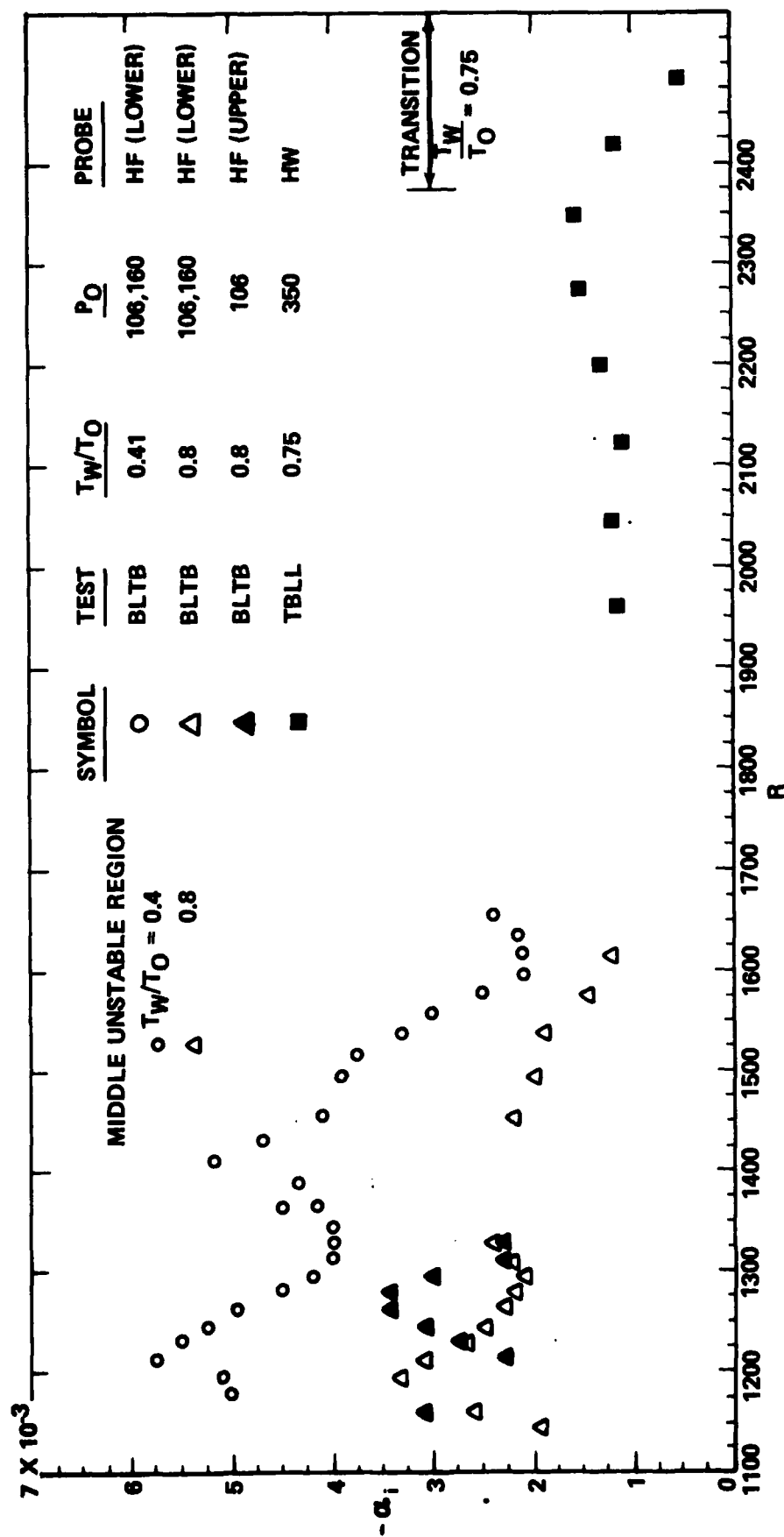


Figure 19. Maximum amplification rates in the middle unstable region. Contributing modes are unknown.

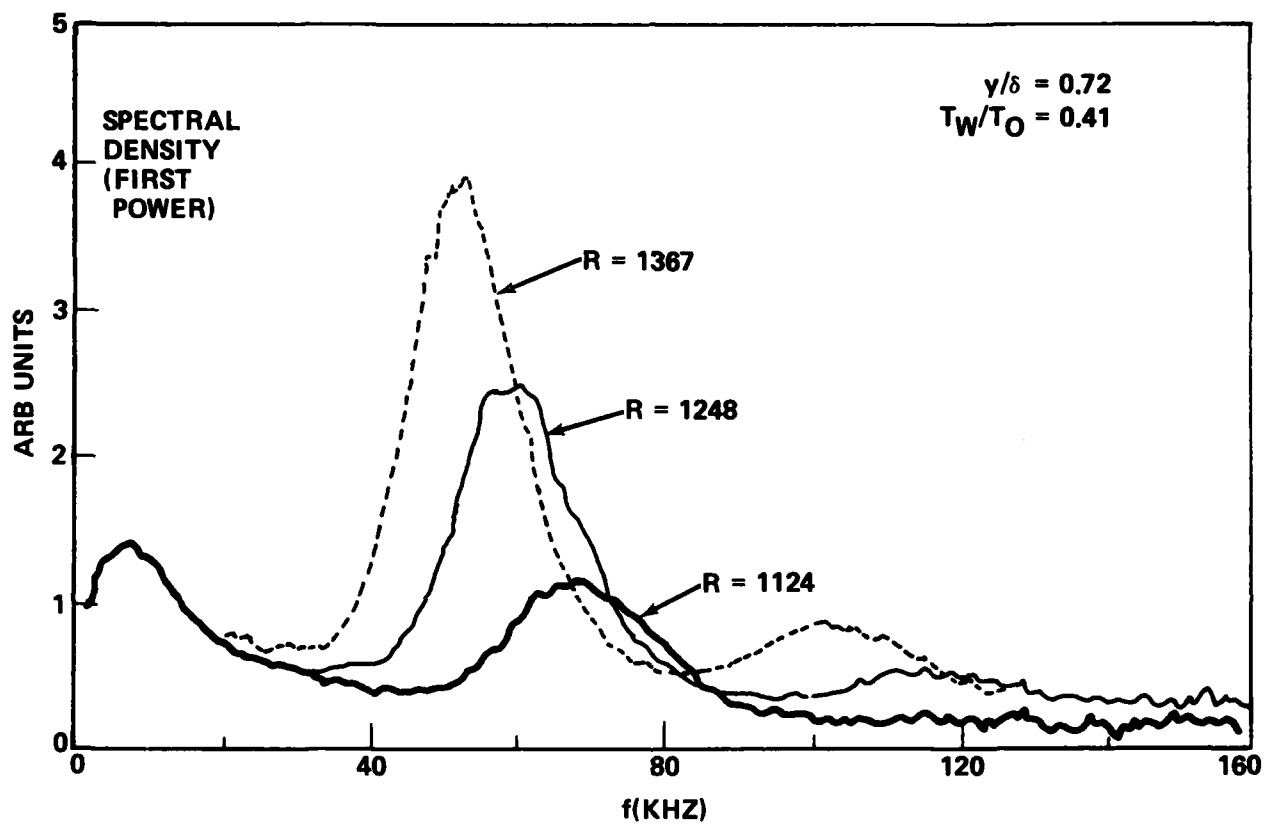


Figure 20. Amplitude spectra (typical).

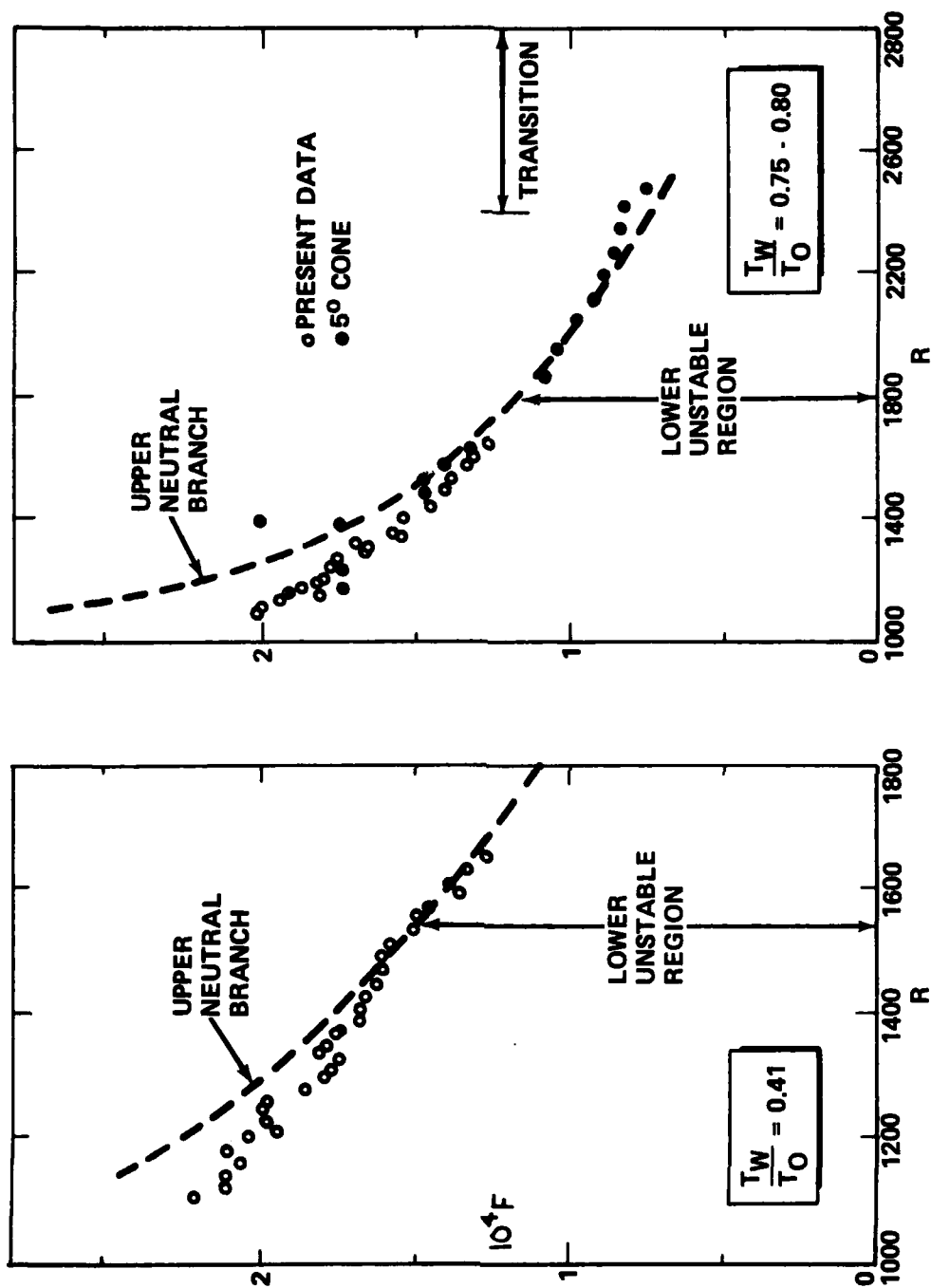


Figure 21. Maximum amplitude lines (of the laminar waves) and their relation to the upper neutral branch of the lower unstable region. Laminar waves damp beyond the crossing point.

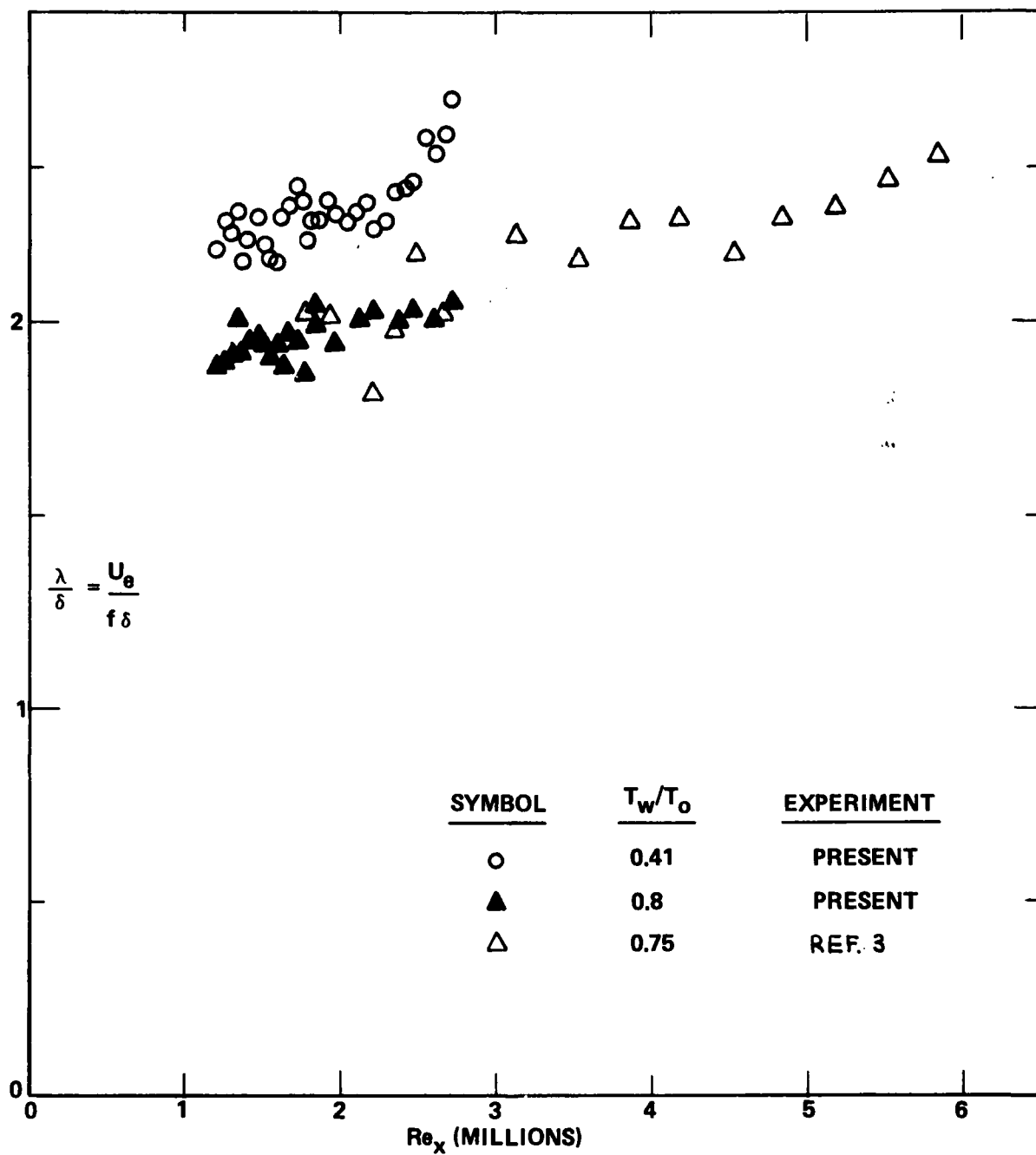


Figure 22. Length of the laminar waves compared to the boundary layer thickness δ . Note slight increase with streamwise distance and lowered surface temperature.

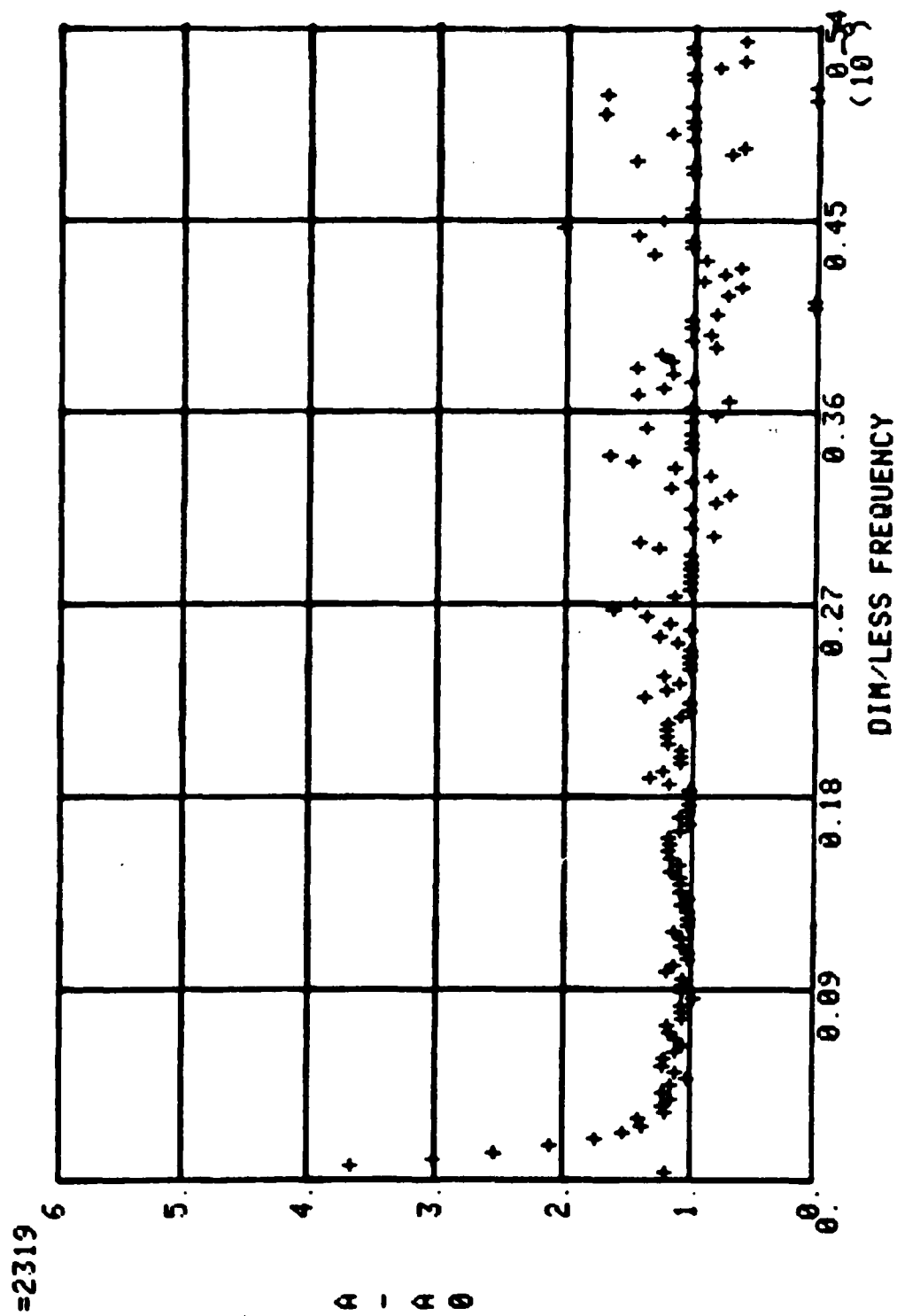


Figure 23. Boundary layer response (TBL, $R = 1166$, $P_o = 150$ psia).

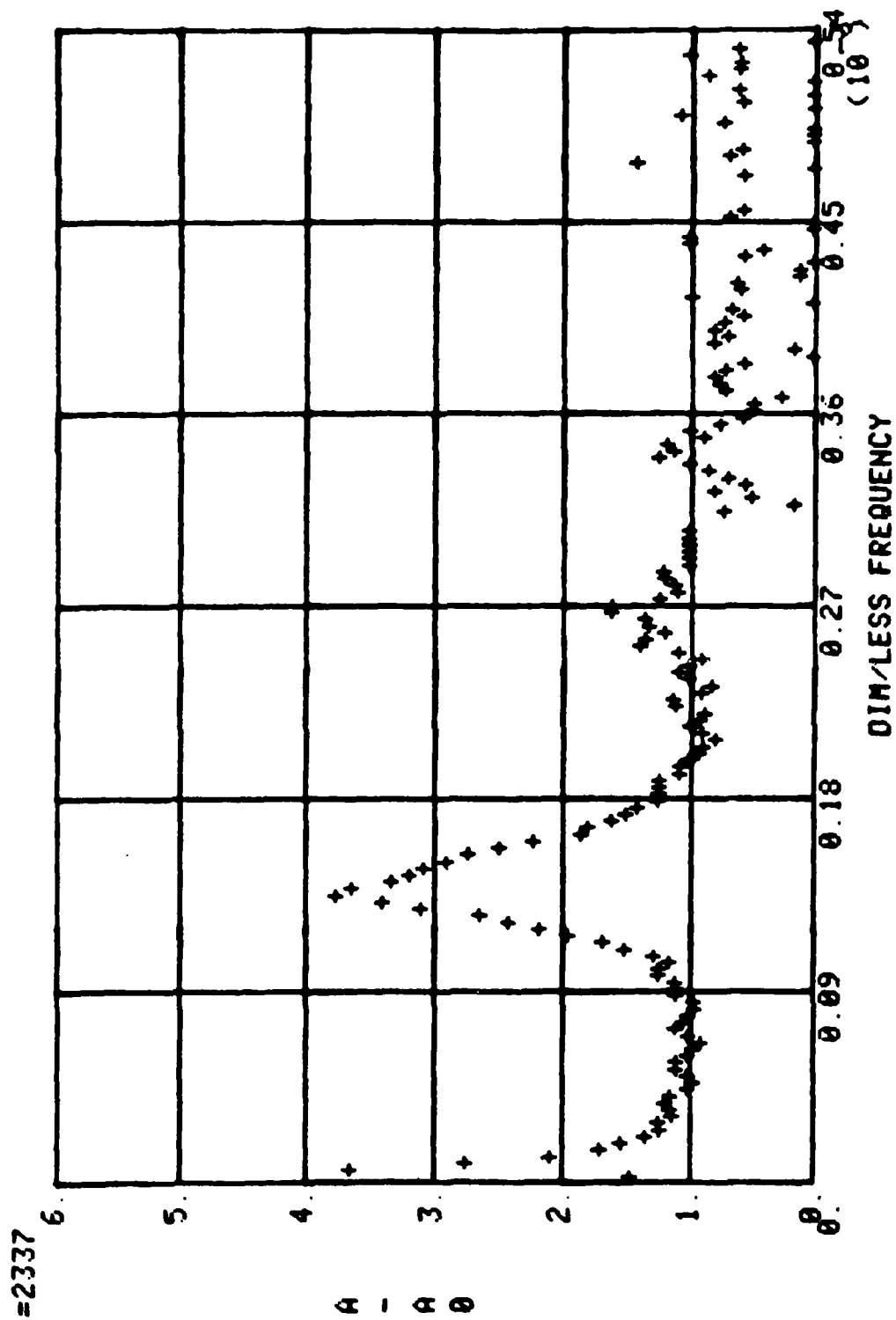


Figure 24. Boundary layer response (TBL, $R = 1628$, $P_o = 150$ psia).

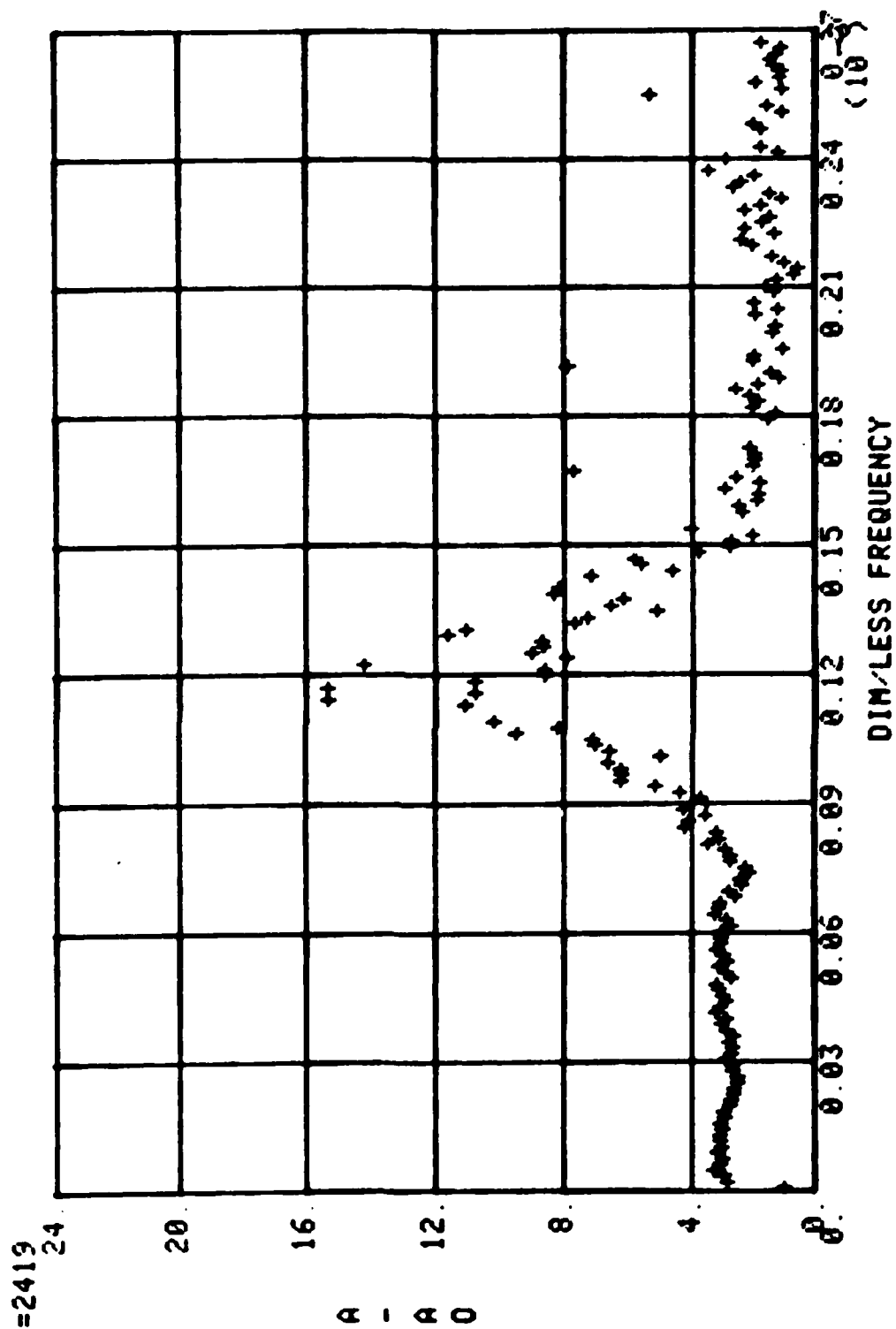


Figure 25. Boundary layer response (TBLC, $R = 1780$, $P_0 = 350$ psia).

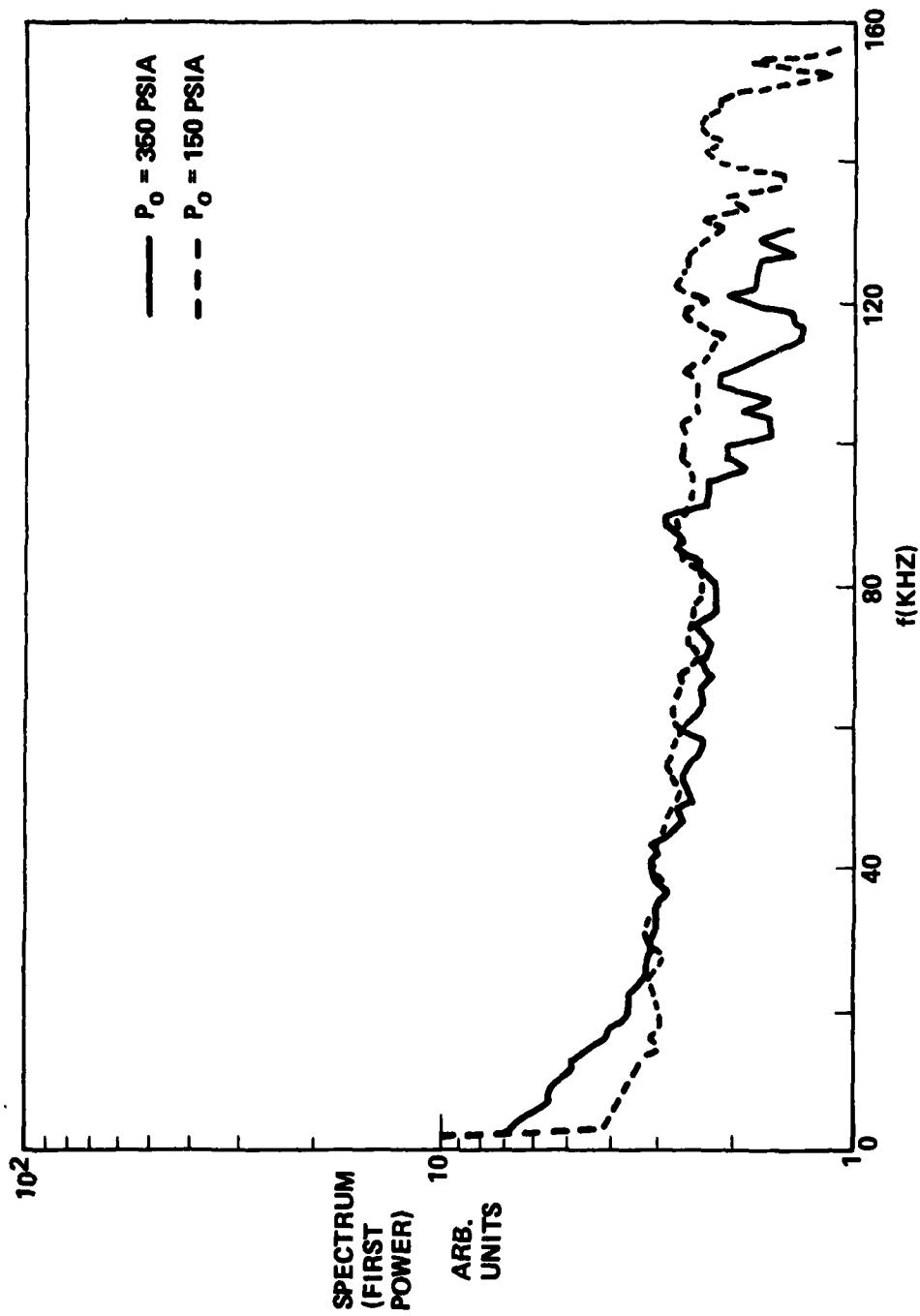


Figure 26. Comparison of freestream spectra at $P_0 = 150$ and 350 psia (TBL-C).

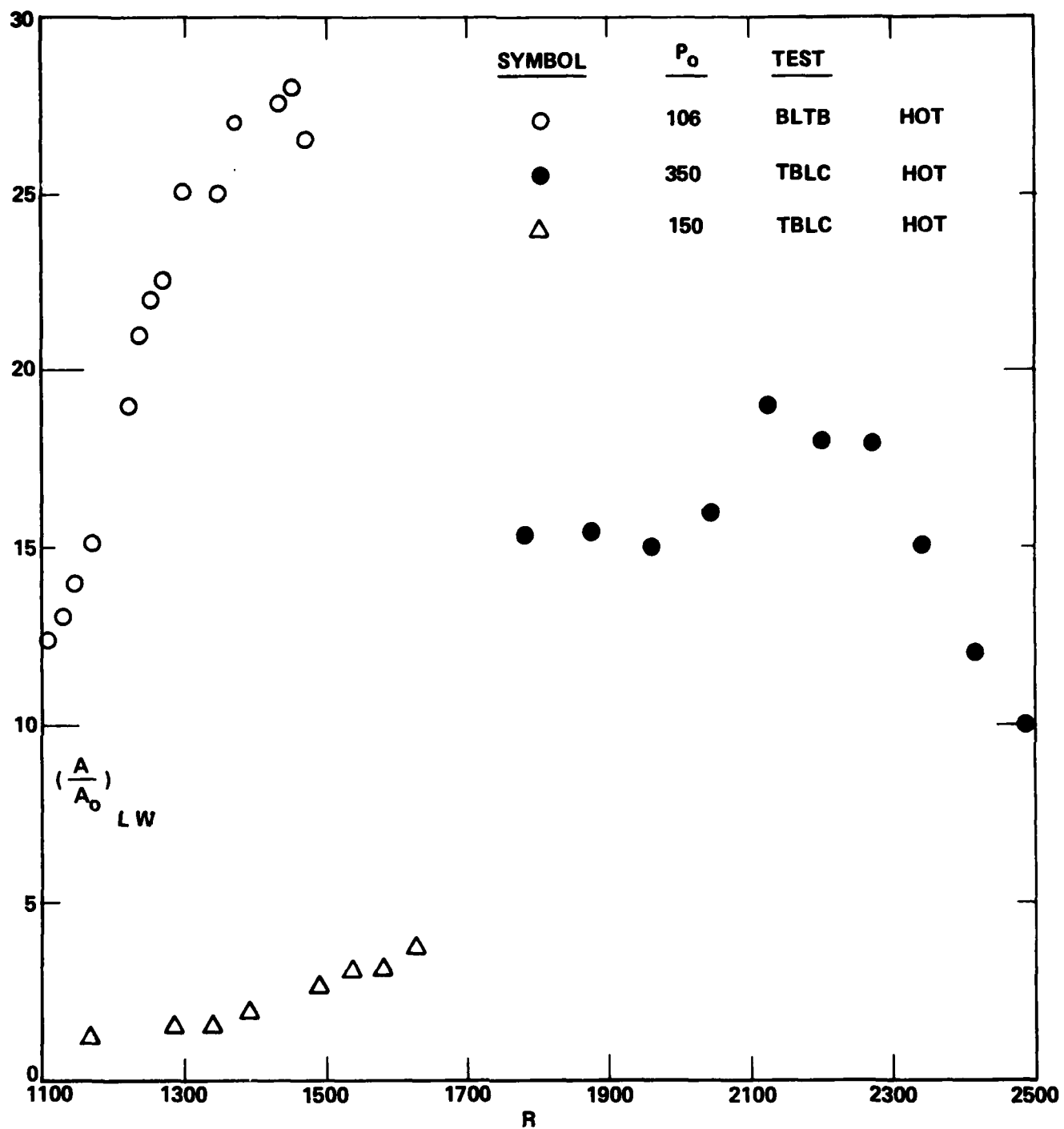


Figure 27. Maximum amplitude of laminar waves referred to the freestream spectrum.

APPENDIX

COMPUTATION METHOD FOR FLUCTUATION DATA

A.1 OVERALL PROCEDURE

The overall procedure is shown on Figure A.1. Each spectrum, consisting of a signal $E(f)$ at frequency f , is played through the TSS into cassette storage. Processing from the cassette then proceeds along two branches: along one branch each spectrum (i.e., spectrum at each R) is first made up into a file SPECXXXX. This file is fed into a program (SPECTRO 1) which gives print-outs of $A(f)$ versus F (or f). If fed into program SPECTRO2, the same file SPECXXXX is re-arranged into file PLOTXXXX suitable for graphics hardware. When called by program TEKPLT,R, plots of $A(f)$ vs f or F can be produced.

The second branch option consists of playing the entire group of digitized spectra (i.e., at a single wind tunnel condition) into the computer to create files ANTHONYX. When played into program STABILIT this file can produce, at any chosen frequency, graphs A vs R or G vs R . As a third option, STABILIT can also plot G vs F for a chosen value of R .

A.2 FILES SPECXXXX AND NOISXXXX

The SPECXXXX files, explained on Table A-I, are the digitized spectra at $y/\delta = 0.72$. To use them, each should be accompanied by the electronic noise file NOISXXXX. In the latter, the digits X of line 120 have the following meaning:

First X: Always 0
Second X: Always 0
Third X: 1 (for $T_w/T_o = 0.8$) or 2 (for $T_w/T_o = 0.41$)
Fourth X: 1 (for $P_o = 106$ psia) or 2 (for $P_o = 160$ psia).

In line 122, each NOISOOXX file has only one number, which is J (the number of points). When using SPECXXXX into programs SPECTRO1 and SPECTRO2, care should be taken to match P_o and T_w/T_o for the SPECXXXX and NOISXXXX inputs: e.g., SPEC11XX goes with NOIS0011 and SPEC21XX goes with NOIS0021.

A.3 PROGRAM SPECTRO1 (BASIC System)

Purpose of this program which is shown on Table A-II, is to produce the variation of $A(f)$ versus f or F in tabular form, for each R . It requires, as inputs, a file SPECXXXX with a matching NOISXXXX. The activating sequence is:

* RUN

WHAT ARE FILES SPECXXXX, NOISXXXX? SPECXXXX
?NOISXXXX

The program then prints out in the format shown on Table A-III.

A.4 PROGRAM SPECTRO2 (BASIC System)

This program, shown on Table A-IV, performs the same function as SPECTRO1, but instead of printing out, it creates files for later use with TSS graphics. The activating sequence is:

*RUN

WHAT ARE FILES SPECXXXX, NOISXXXX, PLOTXXXX? SPECXXXX

?NOISXXXX

?PLOTXXXX

READY

*

These last two lines indicate that a file PLOTXXXX has been written, but saved only temporarily. To save PLOTXXXX permanently, notify the TSS to do so after the BYE command, as follows:

*BYE

X TEMP FILES CREATED

PLOTXXXX? SAVE PLOTXXXX

PLOTYYYY? SAVE PLOTYYYY

etc.

Note the explanation in Table A-IV, since the order of the quantities in the outputted file will be important in plotting graphics.

A.5 FILE PLOTXXXX

This file is typically reproduced in Table A-V for information only since it is usually not printed out. A pair of line statements is used to store the output of SPECTRO2, line 220. Again, the ordering of the PLOTXXXX file is important to remember (see Table A-IV) when running graphics plots.

A.6 USE OF THE TEKPLT,R PROGRAM (FORTRAN System)

This program plots the spectra at each R, as supplied by the PLOTXXXX files created by SPECTRO2. The program itself is permanently stored in the Aerodynamic computer and is too complex to justify its explanation here. The question and answer sequence is shown in Table A-VI, in this example requesting the computer to plot A (f) vs f in KHz for the data group 1129. Examples of the resulting plot are shown in the text.

A.7 FILES ANTHONYX

These files are prepared in order to activate other options in the computation process (see Figure A.1). The ANTHONYX files are simply the entire string of SPECXXXX files for each $P_o - T_w/T_o$ combination, run into the computer at the same time. Thus, there are a total of seven such files created in the present test:

ANTHONY1 for $P_o = 106$, $T_w/T_o = 0.41$ (all SPEC21XX files and NOIS0021)
 ANTHONY2 for $P_o = 160$, $T_w/T_o = 0.41$ (all SPEC22XX files and NOIS0022)
 ANTHONY3 for $P_o = 106$, $T_w/T_o = 0.8$ (all SPEC11XX files and NOIS0011)
 ANTHONY4 for $P_o = 160$, $T_w/T_o = 0.8$ (all SPEC12XX files and NOIS0012)
 ANTHONY5* for $P_o = 106$, $T_w/T_o = 0.8$ (all SPEC55XX files and NOIS0055)
 ANTHONY7** for $P_o = 150$, $T_w/T_o = 0.75$ (all SPEC23XX files and NOIS0023)
 ANTHONY8** for $P_o = 350$, $T_w/T_o = 0.75$ (all SPEC24XX files and NOIS0024)

To prepare each file ANTHONYX it is important to load the cassette in a certain sequence. As presently set up, the line assignments on the cassette must be as follows:

<u>Cassette Line No.</u>	<u>Line No. in Each Group</u>	<u>Type of Data Group</u>
1	120	Noise (NOISXXXX)
2	130 (first datum)	
.....		
200	2110 (last datum)	First spectrum (SPECXXXX)
201	122	
202	120	
203	130 (first datum)	
401	2110 (last datum)	Second spectrum (SPEXXXX)
402	122	
403	120	
etc.	etc.	

Once ready, the cassettes are played into the computer using the EDIT system by the following procedure:

```
SYSTEM? EDIT
OLD OR NEW - NEW
READY
```

*FSHF probe; ANTHONY1-4 is for BLHF probe
 ** TBLC data

ENTER

* # TAPE

READY

(play tape)

CNTRL,X

* CR

- SAVE ANTHONYX

A.8 USE OF THE STABILIT Program

The activation of the STABILIT program is shown on Table A-VII. In this example the curve A vs R is requested at the 116th point in the spectrum.

A.9 SOFTWARE FOR REDUCING TO THE RESPONSE RATIO A/A_o

As shown on Figure A.1, this is done by two additional programs, SPECTRO3 and SPECTRO4 (BASIC system). These are structured much like the SPECTRO1 and SPECTRO2 programs discussed previously.

The freestream spectrum FREE99XX (where XX is a code denoting the particular set of test conditions) and its matching noise spectrum NOIS00XX are first combined through the SPECTRO2 program (Section A.4) to give the noise-free freestream spectrum PLOT99XX, i.e., the $A_o(f)$ spectrum. When combined with any PLOTXXXX spectrum into the SPECTRO3 program, this provides noise-free response spectra A/A_o printouts for any boundary layer spectrum. If graphics plots of this printout are desired, then the combination of PLOT99XX and PLOTXXXX occurs via the SPECTRO4 program, creating a file designated AMPLXXXX, which can then be plotted by the usual FORTRAN/TEKPLT,R program.

The SPECTRO3 and SPECTRO4 programs are shown on Table A-VIII.

BEST AVAILABLE COPY

TABLE A-I
SPECXXXX FILES

FORMAT

```
0120 1129
122 106,0.8,29,1105,199,160,0.331E-08,1
0130 +1669,
0140 +0970,
0150 +1148,
0160 +1290,
0170 +1404,
0180 +1462,
0190 +1488,
0200 +1487,
0210 +1488,
0220 +1488,
0230 +1474,
```

Explanation

Line 0120: First Digit: 1 (For $T_w/T_o = 0.8$) or 2 (for $T_w/T_o = 0.41$)

Line 122 :	<u>Order of Number</u>	<u>Symbol</u>	<u>Explanation and Units</u>
	1	P	Total pressure, psia
	2	T	T_w/T_o
	3	X	Distance from cone tip, inch
	4	R	$R = (Re_x)^{\frac{1}{2}}$
	5	J	No. of points in spectrum
	6	K	Frequency range (KHz)
	7	D	$2\pi/u_e Re'_e$
	8	L	Converts counts to volts per wave analyzer filter

Lines 0130 Data (counts)

TABLE A-II
SPECTR01 PROGRAM

```
10 REM SPECTR01
20 FILES F1:F2
30 DIM C(200),C1(200),V(200),V1(200),V2(200),F1(200),F2(200),N(200)
50 PRINT "WHAT ARE FILES SPECXXXX,NOISXXXX";
60 INPUT F1$
70 INPUT F2$
80 FILE #1,F1$
90 READ #1,H,P,T,X,R,J,K,D,L
100 FILE #2,F2$
110 READ #2,H1,J
120 PRINT
130 PRINT
140 PRINT
150 PRINT "SPECTRUM FOR RUN NO."$H
160 PRINT
170 PRINT "P0(PSIA)="$P
180 PRINT "TW/T0="$T
190 PRINT "X (INCHES) ="$X
200 PRINT "R="$R
210 PRINT
220 PRINT
230 PRINT "N","F (KHZ)","NON-DIM F","E(N) (VOLTS)"
240 PRINT
250 FOR N=1 TO J
260 READ #1,C(N)
270 READ #2,C1(N)
280 LET V(N)=L*C(N)
290 LET V1(N)=L*C1(N)
300 LET V2(N)=SQR((V(N)^2)-(V1(N)^2))
310 LET F1(N)=N*(K/J)
320 LET F2(N)=1000*D*F1(N)
330 PRINT N,F1(N),F2(N),V2(N)
340 NEXT N
9999 END
```

BEST AVAILABLE COPY

TABLE A-III
SPECTRO1 OUTPUT FORMAT

READY
♦RUN

WHAT ARE FILES SPECXXXX,NOISXXXX?SPEC1129
?NOIS0011

SPECTRUM FOR RUN NO. 1129

P0(PSIA)= 106
TW/T0= .8
X (INCHES) = 29
R= 1105

N	F (KHZ)	NON-DIM F	E (N) (VOLTS)
1	.8040201	2.66131E-06	631.2971
2	1.60804	5.32261E-06	952.1948
3	2.41206	7.98392E-06	1139.308
4	3.21608	1.06452E-05	1286.118
5	4.0201	1.33065E-05	1381.199
6	4.824121	1.59678E-05	1450.248
7	5.628141	1.86291E-05	1486.257
8	6.432161	2.12905E-05	1482.7
9	7.236181	2.39518E-05	1485.513
10	8.040201	2.66131E-05	1476.455
11	8.844221	2.92744E-05	1467.241
12	9.648241	3.19357E-05	1469.662
13	10.45226	3.45970E-05	1402.77
14	11.25628	3.72583E-05	1353.572
15	12.0603	3.99196E-05	1357.247
16	12.86432	4.25809E-05	1242.903
17	13.66834	4.52422E-05	1170.7

Notes: N: No. of point along spectrum (1 to 199)
F(KHz): Real-time frequency f
NON-DIM F: Non-dimensional frequency F in text
E(N) (VOLTS): A (f)

BEST AVAILABLE COPY

TABLE A-IV
PROGRAM SPECTRO2

```

10 REM SPECTRO2
20 FILES F1;F2;F3
30 DIM C(200),C1(200),V(200),V1(200),N(200),F1(200),F2(200),V2(200)
40 PRINT "WHAT ARE FILES SPECXXXX,NOISXXXX,PLOTXXXX";
50 INPUT F1$
60 INPUT F2$
70 INPUT F3$
80 FILE #1,F1$
90 READ #1,H,P,T,X,R,J,K,D,L
100 FILE #2,F2$
110 READ #2,H1,J
120 FILE #3,F3$
130 SCRATCH #3
140 FOR N=1 TO J
150 READ #1,C(N)
160 READ #2,C1(N)
170 LET V(N)=L+C(N)
180 LET V1(N)=L+C1(N)
190 LET V2(N)=SQR((V(N)^2)-(V1(N)^2))
200 LET F1(N)=N*(K/J)
210 LET F2(N)=1000*D+F1(N)
220 WRITE #3,N,F1(N),F2(N),C(N),V2(N)
230 NEXT N
9999 END

```

In line 220 note sequence:

<u>Order</u>	<u>Symbol</u>	<u>Explanation</u>
1	N	No. of point along spectrum
2	F1(N)	f in KHz (real time)
3	F2(N)	F
4	C(N)	Original input spectrum, counts
5	V2(N)	Noise-free spectrum, volts

Table A-V
FILE PLOTXXX

000010	1,	.8040201,	2.66131E-06,	1669,
000020	631.2971,	1.60804,	5.32261E-06,	970,
000030	2,	2.41206,	7.98392E-06,	1148,
000040	952.1948,	3.21608,	1.06452E-05,	1290,
000050	3,	4.0201,	1.33065E-05,	1404,
000060	1139.308,	4.824121,	1.59678E-05,	1462,
000070	4,	5.628141,	1.86291E-05,	1488,
000080	1286.118,	6.432161,	2.12905E-05,	1487,
000090	5,	7.236181,	2.39518E-05,	1488,
000100	1381.199,	8.040201,	2.66131E-05,	1488,
000110	6,	8.844221,	2.92744E-05,	1474,
000120	1450.248,	9.648241,	3.19357E-05,	1474,
000130	7,	10.45226,	3.45970E-05,	1419,
000140	1486.257,	11.25628,	3.7	
000150	8,			
000160	1482.7,			
000170	9,			
000180	1485.513,			
000190	10,			
000200	1476.455,			
000210	11,			
000220	1467.241,			
000230	12,			
000240	1469.662,			
000250	13,			
000260	1402.77,			
000270	14,			

Table A-VI
USE OF TEKPLT,R PROGRAM

```

SYSTEM ?FORTRAN
OLD OR NEW-NEW
READY
XRUN TEKGRAPHICS/TEKPLT,R

INPUT NAME OF DATA FILE & NO. OF VARIABLES ON IT
=PLOT1129,5
INPUT SEQ #'S OF VARIABLES TO BE PLOTTED(X & Y)
=2,5
LINE OR POINT PLOT(L OR P) ?
=L
ENTER PLOT SYMBOL
=
XENTER PLOT TYPE CODE
0-LINEAR      1-LOGX      2-LOGLOG
3-LOGY        4-POLAR     X-BACKUP
=0
SPECIFY OUTPUT MEDIUM(FILE NAME OR CR FOR TERMINAL)
=
XSTANDARD PLOT(Y,N,S FOR SAME,X FOR BACKUP) ?
=N
PLOT PARAMETERS STORED ON FILE(Y OR N) ?
=N
XSTANDARD PLOT DIMENSIONS(Y,N,S FOR SAME,X FOR BACKUP) ?
=N
LOWER LEFT CORNER OF PLOT(X AND Y, IN INCHES)
=1.5,1.5
PLOT DIMENSIONS(X AND Y, IN INCHES)
=8,5
XAUTOMATIC SCALING(Y,N,S FOR SAME,X FOR BACKUP) ?
=N

```

Table A-VI (continued)

DATA VALUE AT X-ORIGIN, UNITS/INCH IN X
 =0.,20
 DATA VALUE AT Y-ORIGIN, UNITS/INCH IN Y
 =0.,800
 STANDARD AXES(Y,N,S FOR SAME,X FOR NO AXES, FOR BACKUP,D FOR DONE) ?
 =N
 TICK MARKS/INCH ON X AND Y AXES
 =1.,1
 GRID(Y OR N) ?
 =N
 AXIS INTERSECTION(X AND Y, IN INCHES)
 =1.5,1.5
 STANDARD LABELS(Y,N,S FOR SAME, FOR BACKUP,D FOR DONE) ?
 =N
 X-AXIS LABEL
 =F (KHZ)
 Y-AXIS LABEL
 =S P E C T R A L D E N S I T Y V O L T S
 HORIZONTAL OR VERTICAL LABEL(H,V,D FOR DONE, OR * FOR BACKUP) ?
 =D

TABLE A-VII
ACTIVATION OF THE STABILIT PROGRAM

SYSTEM ?FORTRAN
OLD OR NEW-NEW
READY
*RUN STABILIT

INPUT NAME OF DATA FILE AND NO. OF SIGNALS/DATA SET
=ANTHONY1,199
NOISE EXCEEDS SIGNAL FOR R NO. 7,N= 1
NOISE EXCEEDS SIGNAL FOR R NO. 9,N= 1
NOISE EXCEEDS SIGNAL FOR R NO. 10,N= 1
NOISE EXCEEDS SIGNAL FOR R NO. 1,N= 164
NOISE EXCEEDS SIGNAL FOR R NO. 6,N= 180
NOISE EXCEEDS SIGNAL FOR R NO. 4,N= 190
COMPUTATIONS COMPLETED
INPUT PLOT TYPE(1=CURVE FIT,2=G VS R,3=G VS F,0=STOP)
=1
INPUT DESIRED VALUE OF N
=116

TABLE A-VIII
THE SPECTRO3 AND SPECTRO4 PROGRAMS

```

10 REM SPECTRO3
20 FILES F1;F2
30 DIM N(200),F1(200),F2(200),V2(200),S(200),C(200),S2(200)
40 PRINT "WHAT ARE FILES PLOTXXXX,FREEXXXX";
42 INPUT F1$
47 INPUT F2$
50 PRINT
60 PRINT
70 PRINT "N","F(KHZ)","NON-DIM F","A/A0"
75 PRINT
100 FILE #1,F1$
110 FILE #2,F2$
120 FOR N=1 TO 199
130 READ #1,N,F1(N),F2(N),C(N),V2(N)
140 READ #2,N,F1(N),F2(N),S(N),S2(N)
160 PRINT N,F1(N),F2(N),V2(N)/S2(N)
170 NEXT N
9999 END

```

```

10 REM SPECTRO4
20 FILES F1;F2;F3
30 DIM N(200),F1(200),F2(200),V2(200),S(200),C(200),S2(200)
40 PRINT "WHAT ARE FILES PLOTXXXX,PLOT99XX,AMPLXXXX";
42 INPUT F1$
47 INPUT F2$
48 INPUT F3$
50 PRINT
60 PRINT
75 PRINT
100 FILE #1,F1$
110 FILE #2,F2$
112 FILE #3,F3$
119 SCRATCH #3
120 FOR N=1 TO 199
130 READ #1,N,F1(N),F2(N),C(N),V2(N)
140 READ #2,N,F1(N),F2(N),S(N),S2(N)
160 WRITE #3,N,F1(N),F2(N),V2(N)/S2(N)
170 NEXT N
9999 END

```

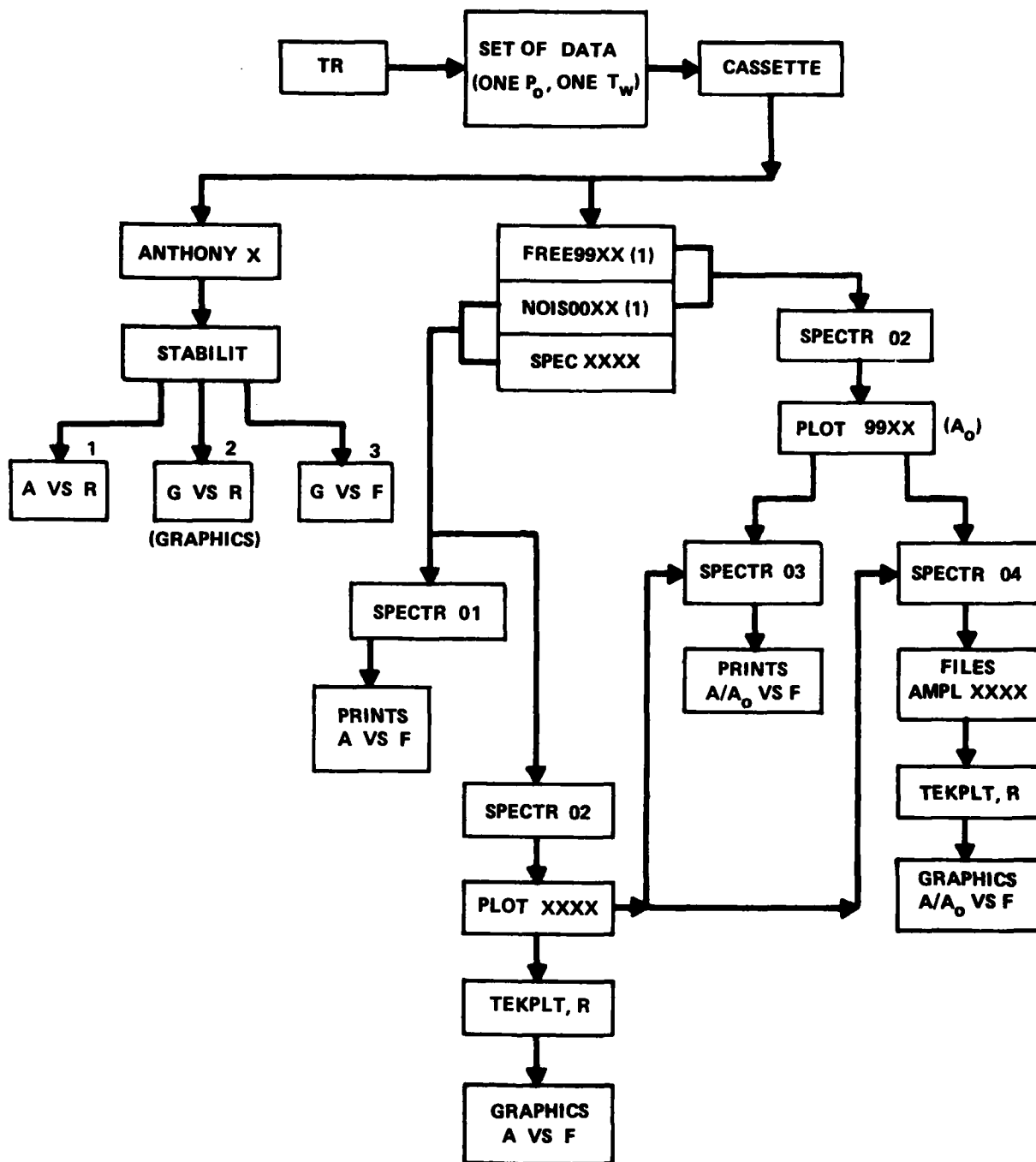



Figure A.1. Diagram of computations used for data reduction.